Problems of Planetology, Cosmochemistry and Meteoritica

Alexeev V.A., Ustinova G.K. Meteoritic evidence on peculiarities of the contemporary solar cycles

V.I. Vernadsky Institute of Geochemistry and Analytical Chemistry RAS, Moscow

Abstract. The meteorite data on monitoring of the intensity and gradient of the galactic cosmic rays (GCR) in the heliosphere during 5 solar cycles are used for the correlative analysis with the variations of the solar activity (SA), strength of the interplanetary magnetic field (IMF) and tilt angle of the heliospheric current sheet (HCS). The dependence of the GCR modulation depth in the 11-year solar cycles on the character of the solar magnetic field (SMF) inversions in the heliosphere at the change of the 22-year magnetic cycles is revealed.

Key words: galactic cosmic rays, solar modulation, solar cycles, inversion of magnetic field, solar dynamo, climate.

Citation: Alexeev, V.A., G.K. Ustinova (2013). Meteoritic evidence on peculiarities of the contemporary solar cycles. *Vestnik ONZ RAN,*

Cosmogenic radionuclides in meteorites: Cosmogenic radionuclides with different $T_{1/2}$, which are observed in meteorites, are natural detectors of cosmic rays along the meteorite orbits during ~1.5 $T_{1/2}$ of the radionuclides before the meteorite fall onto the Earth. The investigation of radionuclides with different $T_{1/2}$ in the chondrites with various dates of fall, which have various extension and inclination of orbits, provides us with such long sequences of homogeneous data on variation of the GCR intensity and integral gradients (E >100 MeV) in the 3D heliosphere [Lavrukhina,Ustinova,1990]. The long sequences of homogeneous data on the GCR intensity in the stratosphere [Stozhkov et al., 2009] are used for evaluation of the gradients. Nowadays, such a sequence of certain homogeneous data on the GCR intensity and gradients in the inner heliosphere covers ~5 solar cycles (see figure 1) [Alexeev, Ustinova, 2006]. This smoothes, to a considerable extent, both the temporal and spatial GCR variations revealing the most important general regularities (curve 1), namely: the dependence of the GCR gradients in the inner heliosphere (at 2–4 AU from the Sun) on the phase of the solar cycles and the constancy of the mechanism of the solar modulation of GCRs, at least over the last ~1 Ma.

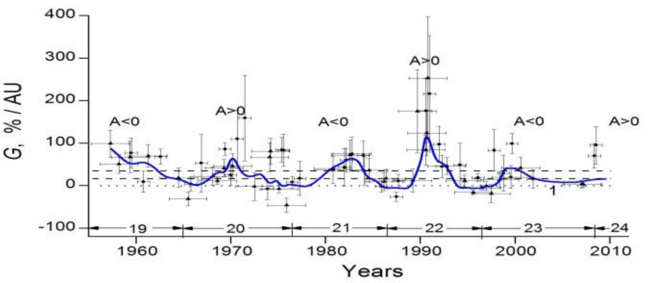

Fig 1. Distribution and variations of the GCR integral gradients G in 1954–2009 along the orbits of the fallen chondrites. The curve 1 fits experimental data by a first-order polynomial based on five points with taking into account the weight of each point

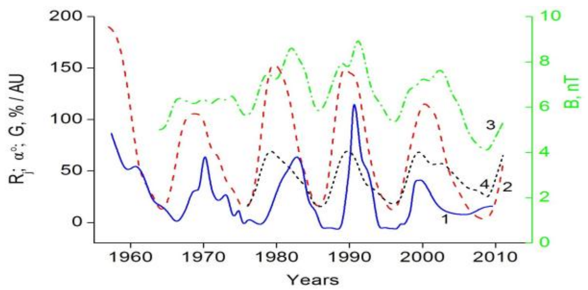

Fig. 2. Variations of GCR gradients (curve 1 from figure 1) in comparison with variations of SA (Wolf numbers R_j), strength B of IMF and tilt angle α of HCS (curves 2-4, respectively) for 1957-2009

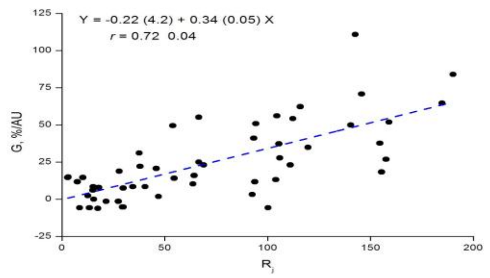

Fig. 3. GCR gradients G (points) vs. R_j in 1957-2009; dashed line is linear regression; correlation factors are pointed out on the graph

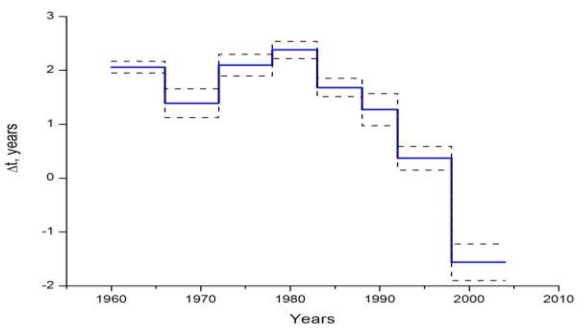

Fig. 4. Change of time lags of variations of the GCR integral gradients from the variations of SA for the considered time scale

Correlative analysis of the data on GCR gradients with the parameters of SA, IMF and HCS: The existence of scaling in the power of the interplanetary magnetic field fluctuations [Burlaga, Ness, 1998] leads to necessity of separation of the stochastic effects and the effects caused by the solar activity (SA) in modulation of GCRs. In this connection, rigorous analyses of correlations between the distribution and variations of GCRs and various indexes of SA, as well as the strength of interplanetary magnetic fields (IMF) and the title of the heliospheric current sheet (HCS) in the three-dimensional heliosphere, turn out to be of paramount importance. Figure 2 shows variations in GCR radial gradients in comparison with variations in the SA [ftp://ftp.ngdc.noaa.gov/STP/SOLAR_DATA/], in the IMF strength [http://nssdc.gsfc.nasa.gov/omniweb/form/dx1.html] and in the HCS tilt angle [http://wso.stanford.edu/Tilts.html]. One can see the positive correlation of GCR radial gradients at 2 - 4 AU with the SA, as well as with the strength of IMF and the HCS tilt angle up. However, the correlation differs for various solar cycles, as well as for growth and decay phases of solar cycles. Indeed, along with general positive correlations of the gradients with the level of SA (figure 3), there are time lags, Δ*t*, of the gradient variations from R_j variations (figure 4). It is apparently determined by the dynamic of accumulation and dissipation of a modulating layer of magnetic irregularities at 2-4 AU from the Sun in the different phases of SA [Lavrukhina,Ustinova,1990]. It is seen in figure 4 that Δ*t* values vary in the range of ~ 1.27-2.38 years (with correlation coefficients >0.9) up to the maximum of the 22nd solar cycle, and then they drop rapidly down, even to negative values (perhaps, due to the SA decrease that started in the following years). It is also interesting that there exists a of considerable north-south (N-S) asymmetry of GCR distributions in 3D-heliosphere at the different stages of SA, which follows from analysis of the data [ftp://ftp.ngdc.noaa.gov/STP/SOLAR_DATA/] on the green coronal lines [Alexeev, Ustinova, 2006], and which is confirmed, e.g., by values of the latitudinal GCR gradients (E > 100 MeV) in 1973–1976 (derived from the radionuclide contents in the Dhajala and Innisfree chondrites with known orbits): G_θ is ~ 3–5% per degree in S-latitudes and from –1.5 to 0.8% per degree in N-latitudes [Lavrukhina, Ustinova, 1981].

3. Influence of the SMF inversions on depth of the GCR modulation: Violation of correlations of the GCR gradients with SA might be conditioned by the disturbance of the SA itself by stochastic processes, e.g., first of all, by the processes of inversion of the total solar magnetic field (TSMF) during the maximum phases of the solar cycles [Ustinova, 1983]. Under the polarity replacement from – to + in the N-hemisphere, the positive phase (A>0) of the 22-year magnetic cycle begins. After passage of the negative phase (A<0), when + replaces – during the maximum of the next solar cycle, the beginning of the new magnetic cycle starts. The TSMF inversion periods differ in their character and duration in N- and S-hemisphere of the Sun for various solar and magnetic cycles [http://wso.stanford.edu/Polar.html]. Indeed, according to [Howard, 1974], in the 20 solar cycle the inversion began developing in March 1968 at heliolatitudes of 40°–50° in the S-hemisphere, and propagated slowly towards the pole, which was reached in September 1969. In the N-hemisphere, the inversion started in the 40°–50° zone only in August 1970, but it was stronger and reached the pole within one year. No inversion occurred in the ±40° equatorial zone in 1969, so that charged particles could penetrate the heliosphere in S-latitudes along the magnetic field lines not only from the polar side but also in the near-equatorial zone at ≤ 40° S [Ustinova, 1983]. In N-latitudes, charged particles had such an opportunity only starting from August 1970 and, especially, in 1971, when the polarity of the magnetic field changed at the N-pole. This means that since September 1969 both the poles were negative for about two years. Thus, owing to the TSMF inversion, the heliosphere proved to be open not only near the poles but also partly in the near-equatorial zone at ±40°. This additional possibility for the penetration of charged particles into the heliosphere through some kind of holes in the magnetosphere was probably responsible for the rapid increase in GCR intensity at the end of 1971 and for the general higher level of GCR intensity in solar cycle 20 as compared with cycle 19 [2]. In fact, TSMF can probably have such configurations when, instead of a single neutral current sheet, there is one neutral sheet and two neutral cones at heliolatitudes of ±40°, which may play a key role if the processes of drift are predominant [Jones, 1983].

Meanwhile, the character of TSMF inversion at the replacement of the magnetic cycle during the maximum of the 22 solar cycle essentially differed from that in the 20 cycle, and it was opposite to it in some details. The fact is that the inversions terminated earlier in the S-hemisphere, at the maxima of solar cycles 18, 19, and 20, and in the N-hemisphere they terminated at the maxima of solar cycles 21 and 22 [http://wso.stanford.edu/Polar.html]. This is related to the fact that during seven 11-year cycles, up to cycle 20 inclusively, the activity in the N-hemisphere was higher than in the S-hemisphere [Vitinskii, 1983]; however, since 1981 the S-hemisphere became more active than the N-hemisphere. At the maximum of the 21 solar cycle the TSMF inversion from + to – terminated earlier in N-hemisphere (02. – 11. 1979) vs. (09.1979 – 05. 1980) in S-hemisphere, and its duration, as a whole, was less than a year, so that such a short-term TSMF deviation from dipole was not especially displayed. However, at the maximum of cycle 22 the inversion from – to + in N-hemisphere covered the range of (01.1989 – 03.1990), which was considerably shorter than the inversion period of (08.1989 – 05.1991) from + to – in S-hemisphere. Hence, some period should exist when both the poles were positive. It means that the heliosphere was closed for positively charged particles, except for two neutral cones with high inclination. That resulted in the deepest minimum of the GCR intensity in stratosphere in 1990-1991 [Stozhkov et al., 2009] and the highest GCR gradients for the 22nd solar cycle (see figure 1).

At last, the 23 solar cycle is considered to be unusual because of very low amplitude of SA and prolonged minimum before the development of the 24 solar cycle [Ishkov, 2010]. The TSMF inversion from + to – in N-hemisphere took place during about one year (11.1999 – 10.2000), whereas in S-hemisphere the inversion from – to + lasted for about 2 times longer (06.1999 – 06.2001), so that the period when both the poles turned out to be negative (as well as in the 20 cycle), was prolonged enough. With the decline of the IMF, observed since 2000, the heliosphere turned out to be still more open for GCR penetration, which is confirmed by the decrease of their gradients (see figure 1). The weakness of the magnetic fields as well as the unusual duration of the SA decline before the 24 solar cycle testify to the transformation of the magnetic field generation in the convective zone of the Sun [Ishkov, 2010; 2012, etc.], which becomes more and more evident with the development of the 24 solar cycle. In particular, in 2008-2009 the IMFs were so weak that the fluxes of particles with energy being less than a few GeV were recorded in stratospheric measurements, which never occurred before [Bazilevskaya et al., 2011].

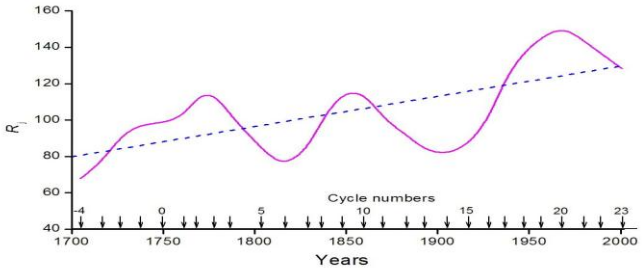

Fig. 5. Secular cycles of SA in 1700–2001 (solid curve is a variation of the maximum annual average Wolf number R_j smoothed by the Gleisberg method; the maxima of the cycles are marked by arrows; the dotted line is a regression line $y = -203 + 0.166x$.

4. Secular cycles, solar dynamo and climate: In contrast to the 11-year cycles connected with the frequency of SA phenomena, the secular cycles reflect mainly variations in their intensity, and thus they allow us to judge about the state in the convective zone of the Sun [Vitinskii, 1983]. It is clearly seen in figure 5 that just with the 20 solar cycle the decrease of the current secular cycle has begun, and nowadays we are at – or approach to – its minimum, which may evidence the decrease of depth of the convective zone of the Sun. The turbulent convection of the solar plasma and its differential rotation underlie free-running operation of the solar dynamo [Zeldovich, Ruzmaikin, 1987]. When some conditions of generation of convection are disturbed, or interaction of the convection with the differential rotation is disturbed (e.g., due to viscosity), states of instability can arise, the ambiguity of going out from which leads to failure of the solar dynamo operation. Then the prolonged minima of SA, being similar to the Maunder minimum, are coming. Nowadays, there is, apparently, just such a trend of events. It will depend, to a large extent, on the character of the inversion in the 24 cycle, which is expected in ~2014 [Ishkov, 2012]. Cycle 24, being similar to cycle 22, must pass through the stage when both the poles will be positive, but it cannot last for a long time. For instance, at low SA the magnetic fields near the poles can be only neutralized, but the inversion will not take place. The disappearance or extreme weakness and instability of the magnetic fields near the poles will open free penetration of GCRs into the heliosphere. The exit from such a state of instability can depend on its duration. In the protracted case, when toroidal, axisymmetric field will be developed near the equatorial zone, a prolonged minimum of SA can come as well as a cold period on the Earth, which is conditioned by it. According to many authors (see, e.g., [Alexeev, 2007]), SA together with the greenhouse effect is the possible causes of the observed global warming on the Earth. However, the superposition of the cycles of various duration and their disturbance demonstrate the complexity and ambiguity of this mechanism. As seen from figure 5, the replacement of every successive secular cycle occurs at the higher level of the solar activity (see the regression line). This means that the more prolonged cycle (perhaps, 400- or 600- year cycle) is on the rise, and just it may be one of the reasons of the observed global warming on the Earth. The future will show whether this tendency to warming will endure a competition with cooling through stochastic turning-off (or attenuation) of the SA cycles or not.

This work is supported in part by the Program No. 22 of Fundamental Research of Russian Academy of Sciences.

References:

1. Alexeev. V.A. (2007). Some features of climate change on Earth and its possible relation to solar-activity variations. *Solar System Res*., 41, No. 6, pp. 527–534.
2. Alexeev, V.A., G.K. Ustinova (2006). Solar Modulation of Galactic Cosmic Rays in the Three_Dimensional Heliosphere According to Meteorite Data. *Geochem. Intern*., 44, pp. 423–438
3. Bazilevskaya, G.A., M.B. Krainev, V.S. Makhmutov, A.K. Svirzhevskaya, N.S. Svirzhevsky, Yu.I Stozhkov (2011). Peculiarities of cosmic ray modulation in the minimum between the 23rd and 24th solar cycles. *Bull. RAS, Physics*, 75, pp. 782–785.
4. Burlaga, L.F., N.F. Ness (1998). Magnetic Field Strength Distributions and Spectra in the Heliosphere and Their Significance for Cosmic Ray Modulation: Voyager 1,1980-1994. *J. Geophys. Res. A,* 103, No. 12, pp. 29719-29732.
5. Howard, R. (1974). Studies of Solar Magnetic Fields. *Solar Phys*. 38, No. 2, pp. 283-299.
6. Ishkov, V.N. (2010). The hydromagnetic dynamo as the source of planetary, solar, and galactic magnetism. *Sun and Geosphere*, 5, No. 2, pp. 43-46.
7. Ishkov, V.N. (2012). http: www.wdcb.ru/stp/cyc24.doc
8. Jones, F.C. (1983). Rapporteur Paper for Sessions MG1, MG3, and MG4. Modulation Theory, Interplanetary Propagation, and Interplanetary Acceleration. *Proc. 18th ICRC, Bangalore,* 12, pp. 373-388/
9. Lavrukhina, A.K., G.K. Ustinova (1981). Galactic Cosmic Ray Gradients in the Ecliptic Plane and at High Latitudes during Two Solar Cycles (Meteorite Data). *Adv. Space Res*., 1, No.3, pp. 143-146.
10. Lavrukhina, A.K., G.K. Ustinova (1990). Meteorites as Probes of Cosmic Ray Variations (Moscow: Nauka)
11. Stozhkov, Yu.I., N.S. Svirzhevsky, G.A. Bazilevskaya, A.N. Kvashnin, V.S. Makhmutov, A.K. Svirzhevskaya (2009). Long-term (50 years) measurements of cosmic ray fluxes in the atmosphere. *Adv. Space Res*., 44, No. 10, pp. 1124-1137.
12. Ustinova, G.K. (1983). Quasistationary Asymmetry of the GCR Density Distribution in the Heliosphere, *Proc. 18th ICRC, Bangalore*, 10, pp. 71-74.
13. Vitinskii, Yu.I. (1983). *Solar Activity* (Moscow: Nauka)
14. Zeldovich, Ya.B., A.A. Ruzmaikin (1987) The hydromagnetic dynamo as the source of planetary, solar, and galactic magnetism. *Sov. Phys. Usp*., 30, pp. 494–506.

Bagulya[1] A.V., Goncharova[1] L.A., Kalinina[2] G.V., Kashkarov[2] L .L., Konovalova[1] N.S., Okateva[1] N.M., Pavlova[2] T.A., Polukhina[1] N.G., Starkov[1] N.I., Vladimirov[1] M.S. **Fragmentation of the super-heavy galactic cosmic ray nuclei in iron-nikel-silicate medium of pallasites: theoretical estimate of the nucleus-fragments yield**

[1] P.N. Lebedev Physical Institute, RAS, Moscow

[2] V.I. Vernadsky Institute of Geochemistry and Analytical Chemistry, RAS, Moscow

Abstract. The simulation results for high energy (400-1000 MeV/nucleon) super heavy (Z > 75) nuclei fragmentation in their interactions with nuclei from the pallasite medium are presented. Monte-Carlo numerical calculations of the yield of different fragment nuclei were held on base of GEANT4 and Hadr01 programs, takes into account all possible mechanisms of ion passing through the matter. The results are presented with the most informative parameters which characterize the energy loss of the primary beam nuclei along their stopping path in the pre-atmospheric meteorite body, the secondary particle energies and charge distributions.

Key words: galactic cosmic rays, super-heavy elements, pallasite meteorites, nuclear fragments.

Citation: Bagulya A.V., L.A.Goncharova, G.V.Kalinina, L.L.Kashkarov, N.S.Konovalova, N.M.Okateva, N.G.Polukhina, N.I.Starkov, M.S.Vladymyrov (2013). Fragmentation of the super-heavy galactic cosmic ray nuclei in iron-nikel-silicate medium of pallasites: theoretical estimate of the nucleus-fragments yield, *Vestnik ONZ RAN, doi:*

Introduction. The continued track research of the charge spectrum of galactic cosmic ray (GCR) nuclei in meteorite olivine crystals, carried out under the OLYMPIA project [Ginzburg et al., 2005], has led to the need of the introducing the corrections due to the process of fragmentation of primary superheavy nuclei in the meteorite matter under investigations. It is essential that the fragmentation leads to needed of underestimation of the registered number of the primary GCR nuclei and also to increasing in the secondary flux of nuclei as the fragmentation products. There are present in the work the results of the theoretical calculations of the fragmentation effect of the most prevailing in the Solar system nuclei. We are interested the elements in the charge interval of (50<Z<92), as distribution of these nuclei after of interaction with the meteorite matter nuclei indicate higher change in their distribution. The calculations were made with using of the computer simulation of fragmentation process under the program GEANT4 [GEANT4 Collaboration, 2003]. There have been modeled the following variants of nuclei passing: (1) through $Fe_{0.9}Ni_{0.1}$ targets with thickness of 1 cm, 4 cm, 7 cm and 10 cm with the energy values of the primary nuclei from 500 to 1000 MeV/nuclon; (2) through the braking matter of the average chemical composition of pallasite meteorites: 65 vol. % of $(Mg_x, Fe_{1-x})_2SiO_4$ and 35 vol. % of $Fe_{0.7}Ni_{0.3}$. The results obtained enable: (a) to carry out the analysis of the change in composition of output nuclei, produced in the fragmentation process, in different depth from the surface of the irradiated pallasite body, and (b) to quantitatively evaluate the contribution into the nuclei group with Z = 60-75 from the heavier nuclei of GCR elements, which were broken under the fragmentation in the meteorite-pallasite matter.

The research purpose. The model calculations task is primarily based on the contribution calculation of secondary nuclei produced in the fragmentation of primary GCR nuclei, penetrating into the body of the meteoroid and decelerated in olivine crystals of pallasite.

1. Since the highest yield of nuclei, the products of the fragmentation process of the primary nuclei Z_0 can be traced in charge field of secondary nuclei Z_i , close to the Z_0 , as a result, to obtain the most complete picture of charge changes in the GCR nuclei, registered in our tracks research in olivine crystals, which are contained in the iron-silicate braking pallasite matter (stopping medium), it is necessary to calculate and to summarize the contributions of all the most common GCR nuclei.

Table 1. The composition and relative abundance of the most common GCR nuclei for the interval of charges (50-92) in the Solar system [Cameron, 1986].

Element (*)			The content of nuclei (**)
Sn	50	112-124	0.764
J	53	127	1.27
Cs	55	133	0.39
Ba	56	130-138	2.595
Eu	63	151,153	0.047
Ho	67	165	0.092
W	74	180-186	0.079
Ir	77	191,193	0.383
Pt	78	195	0.411
Au	79	197	0.21
Pb	82	207	1.094
U	92	238	0.02

(*) For each element it is given the magnitude of the nucleus charge and the atomic weight of isotopes.
(**) The nuclei content in relation to the GCR VH-group: (^{24}Cr, ^{25}Mn, ^{26}Fe, ^{27}Co, ^{28}Ni), the total content of which is 8.064×10^5 nuclei.

2. The energy of the primary nuclei of E_0 should correspond to the distance traveled by the nuclei in the pallasite matter from the surface to the boundary of the area immediately adjacent to the olivine crystal - tracks detector. This should take into account such geometrical factors, as finding the depth of olivine crystals from the nearest point on the pre-atmospheric surface of the meteoroid. According to the analysis of the distribution of olivine crystals in the GCR VH nuclei tracks density, the depth of the position in the meteorite matter for Eagle Station was (1.5-4) cm, and for Marjalahti (4-8) cm. The sizes of the crystals as the track detectors are 0.5-2 mm.

3. When the tracks are registered in the separate crystals of olivine it is important to know not only how many nuclei are formed in a layer of a certain thickness of meteorite retarding material − the fragmentation products, but how many of these nuclei with a certain threshold energy (corresponding to the tracks formation for olivine crystal) takes off from the surface nickel-iron layer directly adjacent to the olivine crystal detector (registered

under 2π-geometry). In addition, for the certain nucleus (Table 1) from the entire set of incident nuclei of super-heavy GCR elements with using SRIM-program were determined threshold energies at which the nucleus can generate track in the olivine detector contacting the braking matter. The magnitude of this effect can probably be estimated from the flow of GCR nuclei with charge Z_0, which formed the secondary nuclei-fragments at the approach to that olivine crystal, i. e. it must be regarded as an "exit" for the layer of braking matter, the effective thickness of which corresponds to the energy distribution of the nuclei − the products of fragmentation processes.

Thus, the layer thickness, for which the fragmentation is calculated, ultimately is determined on the primary nuclei energy reaching that crystal of the detector tracks and energy of secondary nuclei - products of fragmentation. Thresholds energy of nuclei and their quantity inlet (Fe,Ni) and (Fe,Ni,olivine) targets of different thicknesses, at which remaining after fragmentation nuclei are formed the tracks in contacting olivine crystal detectors, are estimated.

At the first phase of the work the calculations were carried out for evaluation of the "effective" thickness of the nickel-iron layer of about 1 micron, 10 micron and 100 microns, which were selected on the basis of the path lengths of the nuclei with Z >50 at energy of < 1, ~1 and ~10 MeV/nucleon, respectively.

The model calculations. There were simulated total ionization loss and fragmentation of nuclei set in the charge interval of (50-92) with the initial energy of 500 to 1000 MeV/nucleon. Thus, it was accounted the number of the nuclei which passed through the set of thicknesses (10, 40, 70 and 100 mm) of the iron-nickel target, as the part of the meteorite braking matter, $Fe_{0.9}Ni_{0.1}$ with the density of (7.9 ± 0.1) g·sm^{-3}.

Thus, in this model there is analyzed not only the character of changing of " yield " nuclei, the fragmentation products, with the depth from the surface of the irradiated pallasite body, but also the possibility of estimates obtaining of the contribution to the group of nuclei with Z = 60-75 from the nuclei of heavier GCR elements broken in the fragmentation in the meteorite-pallasite matter.

Conclusions. Estimation of fragment nuclei yield after super-heavy GCR nuclei interactions in (Fe,Ni) target shows near of the ~10% output of secondary nuclei with charge in interval of 60 < Z < 75 relatively to initial flux of the more heavy nuclei.

Superposition of the fragment nuclei over GCR nucleus flux in the region 60 < Z < 75 gives up to several tenths of percent which are needed to be taken into account in the track experiments on GCR charge composition investigation.

The work was supported by the RFBR grant №10-02-00375-a and the Program No. 22 of Fundamental Research of Russian Academy of Sciences.

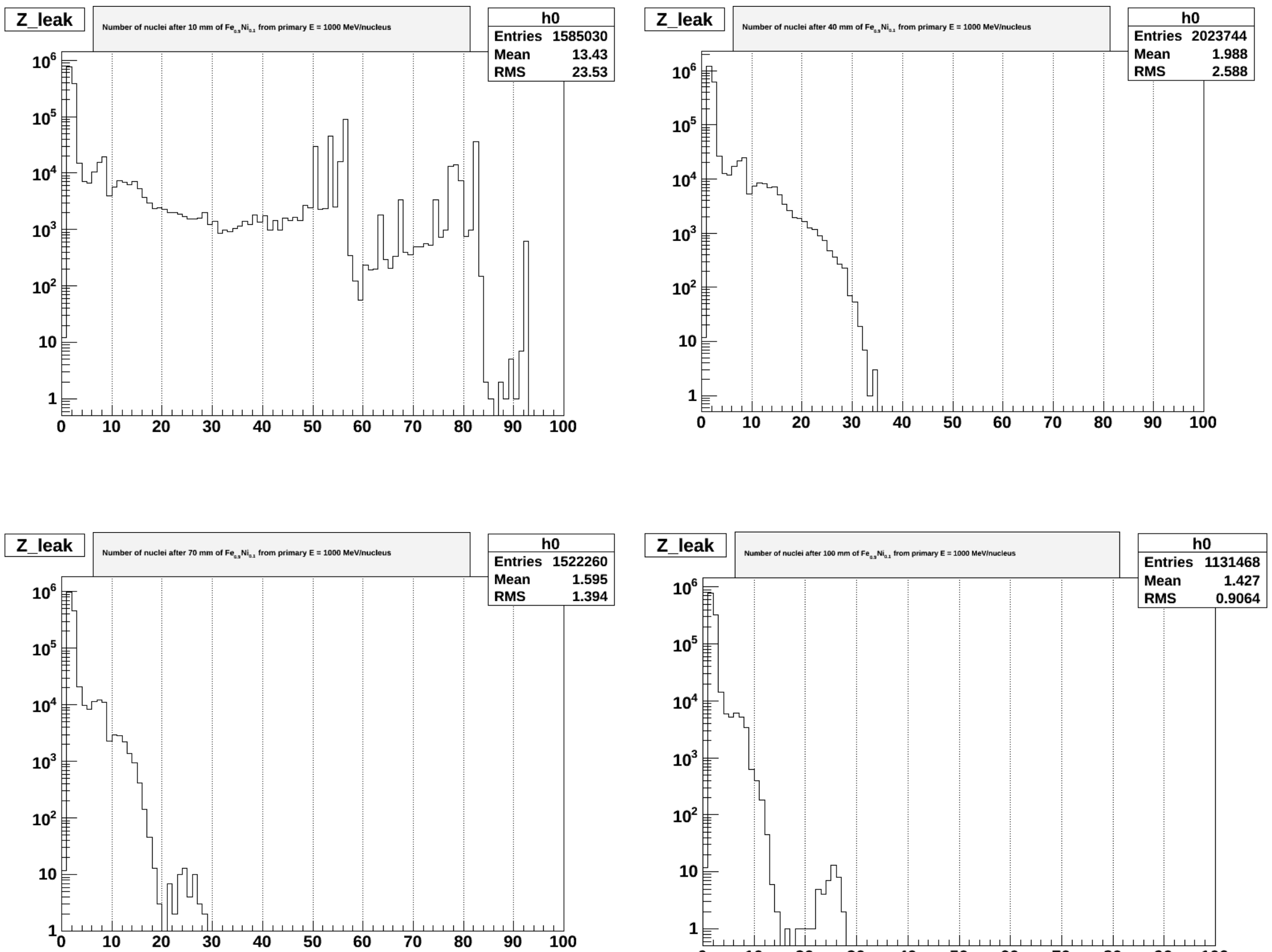

Fig. 1. The spectra of nuclei after the passage of various thicknesses (10, 40, 70 and 100 mm) iron-nickel target for a set of nuclei from the range of charges (50-92) with the initial energy of 1000 MeV/nucleon.

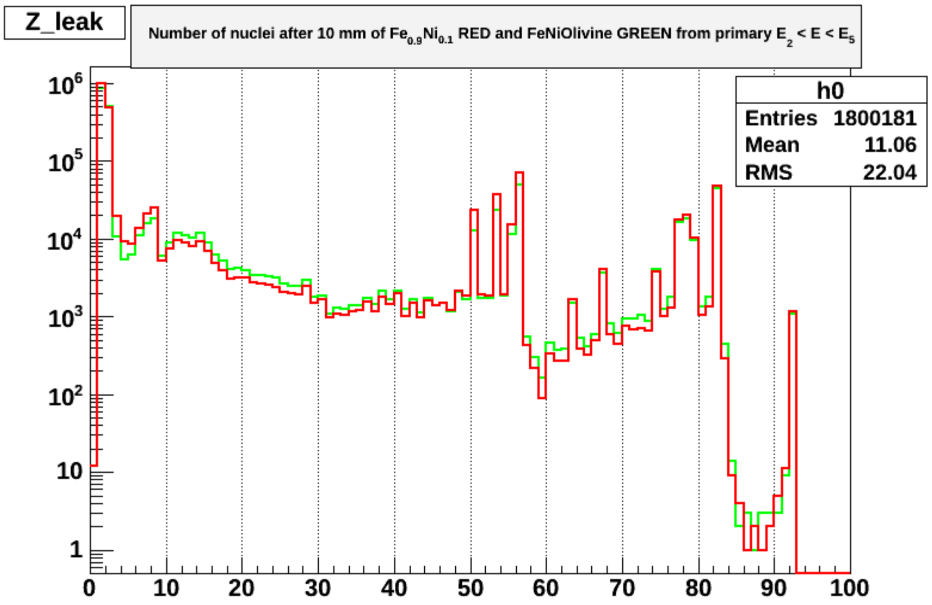

Fig. 2. The charge spectra of the uranium nuclei after passing through {65 vol. % $(Mg_x,Fe_{1-x})_2SiO_4$ and 35 vol. % $Fe_{0.7}Ni_{0.3}$} = (Fe,Ni,olivine) target of 10 mm thick and through {$Fe_{0.7}Ni_{0.3}$} = (Fe,Ni) target of 10 mm thick for nuclei with energy defined by the threshold interval.

References:

1. Cameron A.J.W (1986). Nuclear Astrophysics, ed. Boris C., D. Clayton, J. Schramm. Mir, p. 33-52.
2. GEANT4 Collaboration, S. Agostinelli et al., (2003). "GEANT4: a simulation toolkit, *Nucl. Instr. and Meth.* A506 250 - 303. doi:10.1016/S0168-9002(03)01368-8
3. Ginzburg V.L., N.G. Polukhina, E.L. Feinberg, N.I. Starkov, V.A. Tsarev (2005). Problems and Horizons of the Search for Tracks of Heavy and Superheavy Nuclei in Olivine Crystals from Meteorites (OLIMPIYA project). *Dokl. Physics*. V. 50. № 6. P. 283 – 285.

Barenbaum [1]A.A., Shpekin [2]M.I. Galactic comet fall as a source of water on the Moon

[1]Oil and Gas Research Institute RAS, Moscow
[2]Kazan Federal University, Kazan

Abstract. The amount of water which has arrived at the Moon with the galactic comets during the period from 5 to 1 million years ago is estimated. Fall of these comets quantitatively explain the origin of the present water ice on the Moon. With images of the lunar surface using high-resolution shows evidence of large masses of frozen water in the rocks of the bottom and sides of young comet craters Tsiolkovsky and Aitken. The resulting conclusion: the process of allocation of water in the comet crater continues today.

Key words: water on the moon, galactic comets, craters.

Citation: Barenbaum A.A., M.I. Shpekin (2013). Galactic comets fall as a source of water on the Moon. Bulletin of the Department of Earth Sciences

Introduction. The presence of water on the Moon is established by recent research [Bazilevskii et al, 2012]. In particular, traces of water were found: 1) in igneous rocks delivered from the Moon to the Earth, 2) in the lunar regolith from the IR spectra of the sunlit portions of the lunar surface, and 3) in craters at the lunar poles on measurements of epithermal neutrons.

At present, three groups of hypotheses are proposed to explain the presence of water on Moon.

1. The inflow of juvenile water from the depths at the peak of lunar volcanism 3.2-3.7 billion years ago [Head, Wilson, 1979; Gaddis et al, 1985; etc.], and then later [Hiesinger et al., 2001]. It is estimated [Bazilevskii et al., 2012] that 10^{11}-10^{12} m of water could stand for the outpouring of basalts.

2. Reaction of solar wind protons with regolith and their subsequent conversion to hydroxyl OH, and then H_2O [McCord et al., 2010; McCord, Combe, 2011; Burke et al, 2011]. According to [Housley et al, 1973, 1974; Arnold, 1979] solar wind can form on the surface of the Moon annually 50 tons of water. In this case, the lunar surface is saturated with OH for about ~10^3 years. It is noted that protons can also get to the Moon when it gets to the tail of the Earth's magnetosphere. In this case, the saturation is reached for about ~10^4 years.

3. The fall of the Solar system comets on the Moon [Shevchenko, 1999; etc.], as well as water-rich C-type asteroids [Ong et al, 2010; etc.]. Shevchenko estimated that for the mass of the observed ice deposits on the Moon requires 6×10^4 falls short-period comets or 300 falls of giant comets such as Hale-Bopp. And according to the calculations of Ong and others over the last billion years $(0.13–4.3)\times10^9$ tons comet and 2.7×10^9 tons of asteroidal water could be accumulated. That explains a lot of water ice at the poles, estimated at 2.1×10^8 tons [Feldman et al, 2001].

Paper tasks. In connection with the discovery of the phenomenon of jet expiration of gas and dust material from the galactic center [Barenbaum, 2002, 2010] the main source of water on surface of the Moon is recognized as comets fall of galactic origin. These comets arise in the areas of gas condensation (star) of galactic branches and enter the Solar system solely at the intersection of moving along the galactic orbit of the Sun jet streams and the spiral arms of the Galaxy. The last such period occurred 5÷1 million years ago and was due to staying of the Sun in the jet stream of Orion-Cygnus.

According to [Barenbaum, 2002], these comets had a jet stream velocity relative to the Sun 450 km/s. They consisted primarily of water ice density ≈1 g/cm^3, had a diameter of 100÷3500 m, weight of 10^{12}÷10^{17} g and energy of 10^{20}÷10^{25} J. In the last period of "comet shower" mostly they bombarded the southern hemisphere of the Moon [Barenbaum, 2012], and their falls density was 3-5 bodies of all sizes to the site 100×100 km^2 [Barenbaum, 2012a]. This frequency of galactic comets falls is at least two orders of magnitude larger than the Solar system comets and asteroids of the same size. With an average weight of galactic comets ~10^{14} g only during the last bombardment 5÷0.6 million years ago ~10^{11} tons of water could be brought to the Moon.

It is assumed that some part of cometary water could be preserved in the rocks of the lunar surface [Shevchenko, 1999; Pierazzo, Melosh, 2000; Artemyev, Shuvalov, 2008; Ong et al., 2010]. Theoretically estimate the amount of this water is very difficult [Bazilevskii et al, 2012]. In this paper we show the possibility of bringing to its decision the orbital images of Tsiolkovsky (diameter 180 km) and Aitken (diameter 130 km) craters on the far side of the Moon (Fig. 1).

Both craters have central peaks, and their bottoms are covered with "fresh" basalt lava. Fig. 1**A** arrow indicates the direction of the fall of the galactic comet. At the point of the comet impact (the end of the arrow) on the high-resolution images we have discovered [Shpekin, 2009; Barenbaum, Shpekin, 2011] pouring lava volcano height of 102 m, located on a small flat oval elevation of plume nature 24-26 km in diameter (Fig. 2) .

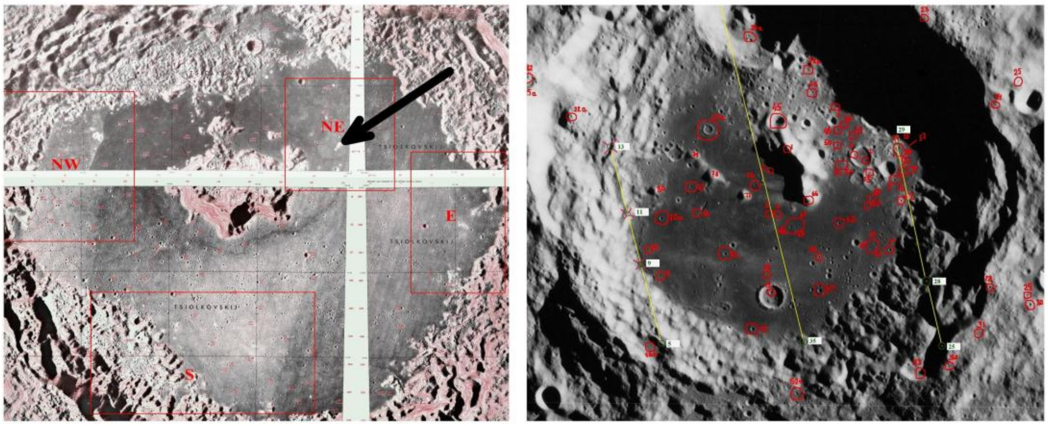

Fig. 1. The outward appearance of Tsiolkovsky crater (left) and the crater Aitken (right). So Tsiolkovsky crater is shown on maps LTO, built in the U.S. based on survey Apollo 15 (1971). The original territory of the crater is presented on 4 sheets of 1:250,000 scale maps. Here, all four sheets are mounted in a single image. The black arrow in the square «NE» shows the estimated direction of the galactic comet, and the end of the arrow rests precisely in the volcano. Aitken crater is represented by one of the soviet "Zond-8" (1970). Here you can see a small piece of the image coated with a label bearing the crater catalogue [Shpekin, Sitdikova, 2007], which was built to study its topography. The lines along which the Clementine (1994) measured by means of onboard laser altimeter [Shpekin et al., 2008] are shown in yellow.

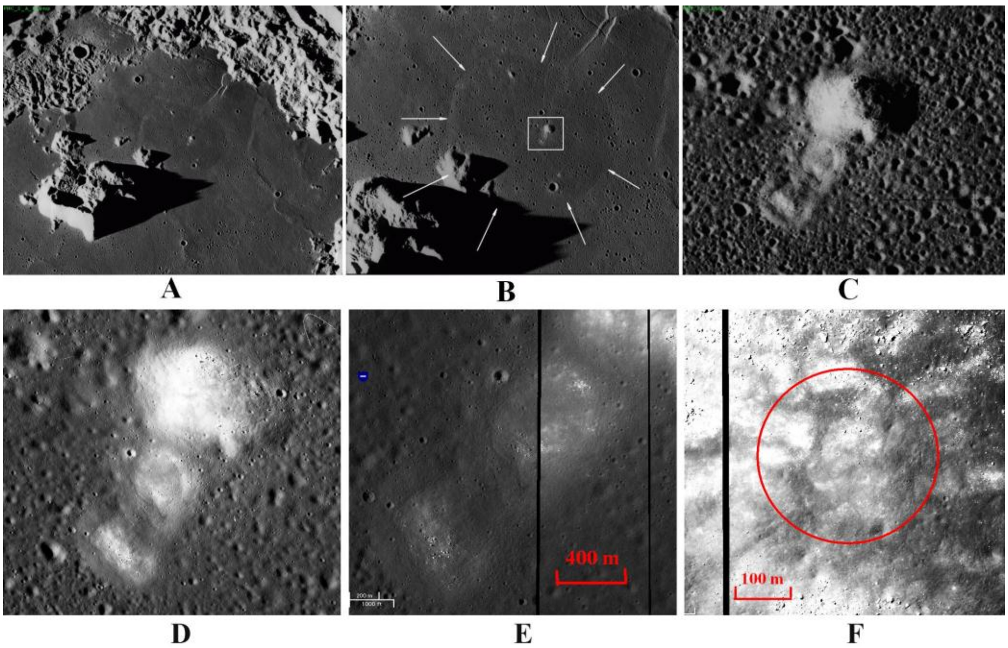

Fig. 2. The volcano view on the bottom of crater Tsiolkovsky on Apollo and LRO images. Fragments A, B and C (1972, image A17-M-2799) show view of the volcano and the surrounding area at a low altitude of the Sun above the horizon, which provides a high contrast and allows to examine the detail of effused volcanic material. Fragments D, E, F are taken from pictures with the worst lighting conditions, but the high resolution allows us to see the structure of effusions: D (1971, image A15-PAN-9594) and E (2011, LRO), F – enlarged view of the central part of the volcano, red circle is the volcano caldera. Images are taken from the digital archives of the Arizona University: http://apollo.sese.asu.edu/, http://wms.lroc.asu.edu/lroc/, http://lroc.sese.asu.edu/images/

The combination of volcanoes and plume rises is typical of the shallow magma chambers, resulting in the fall of galactic comets [Barenbaum, 2013]. We believe that such a chamber volume of ~ 10^2 km^3 now exists under the bottom of the crater Tsiolkovsky.

According to our data and Tsiolkovsky crater Aitken emerged at the last galactic bombardment by comets. Tsiolkovsky crater was formed about ~1 million years ago, and the crater Aitken, probably by about 1–2 million years earlier. Judging by the crater diameters, the comets, which had created the craters, had masses of ~10^{10} tons and ~$3 \cdot 10^9$ tons respectively. If all the comet water remained in the crater, then a layer of ice on the bottom of it would be in the first case, 56 cm, and the second – 35 cm.

It is obvious that the galactic comet is completely destroyed during the crater formation. High resolution images, however, show that the water, which is part of the comet, leaves the crater not completely. Some of the water is captured and frozen in rock walls and bottom of the crater. Over time, thawing, these rocks subsequently recover water, which leads to phenomena previously not discussed in the literature. Three of these phenomena are discussed below.

Actual data. The first phenomenon is the existence of the moving glaciers on the Moon. Fig. 3 are shown as examples of glaciers that descend in the form of a tongue from the south-western slope of a steep central peaks crater Tsiolkovsky and Aitken.

The second fact we associate with the evidence of the existence of the moving water in the surface layer of the Moon. One piece of evidence is a volcano in the crater Tsiolkovsky, pouring, according to Fig. 2 “liquid” lava, with a large amount of water that freezes and rapidly sublimates. Fig. 4 shows another example. This portion of the surface of the crater bottom Tsiolkovsky north central peak on which there are ravines and “frozen rivers”. It is likely that these structures could arise earlier with mobile water.

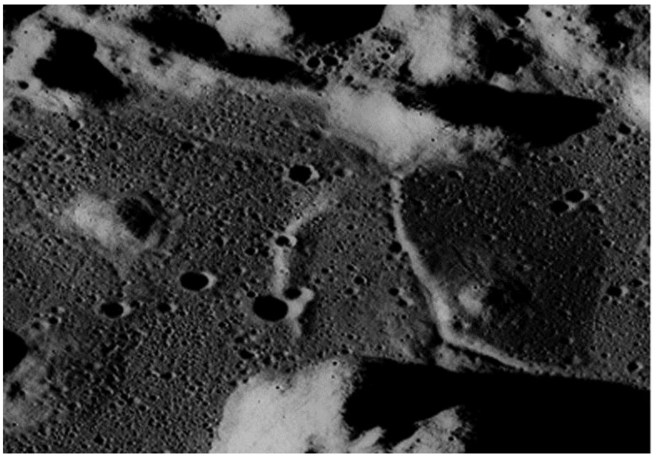

Fig. 4. Ravines and rivers at the bottom of the crater Tsiolkovsky north of the central peak

Fig. 5 illustrates another phenomenon widespread in the crater Tsiolkovsky and associated with the roll-away stones gradually thawing under the regolith slopes of the crater. Note that the resolution of the image allows you to see the stones of the size of ~1 meter. The picture leaves no doubt that the defrosting of covered with a layer of regolith rocks with outcrop containing rock fragments occur nowadays. Expiring in the process stones move out or roll down the slopes, filling the depressions and grooves in relief of the crater wall, or remain in the high regions of the surface with a zero slope. An example is the Fig. 3 (see B and C), where large rocks are concentrated in large number at the top of the ridge, which is seen in the drawing.

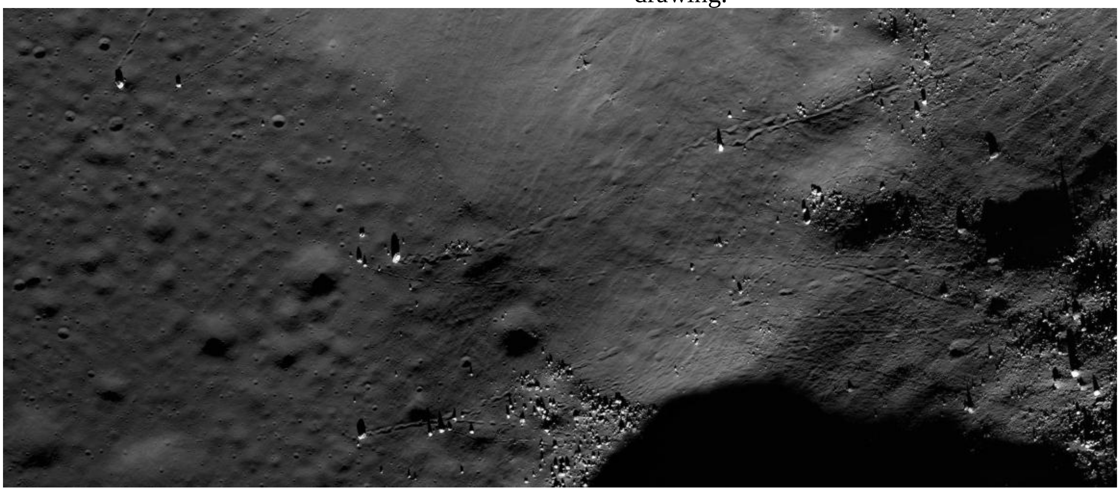

Fig. 5. The latest traces in the lunar regolith, left on the steep slope of the central peak of the crater Tsiolkovsky not yet covered with the lunar dust. Stones, called "boulders", ranging in size from one to several meters, roll down the hill (the bright part of the territory), reaching the bottom of the crater (the dark area on the left of the image), and stay in the horizontal section. Image fragment M115462338RC_pyr.tif of narrow-angle LRO camera from the University of Arizona web-site.

The conclusions

• The main source of water on the Moon, as well as on all the planets [*Barenbaum, 2010*], is cyclic bombardment of the Solar system by galactic comets.

• The amount of water on the Moon can be explained by galactic comets falls in the period from 5 to 0.6 million years ago.

• A significant, but still difficult to define amount of frozen water is present under a layer of regolith rocks in the bottom and sides of large comet craters.

• This water is released in the modern geological processes proceeding on the Moon. The last two questions need special study.

Two final questions are need special study.

References :

1. Artemieva, N.A., V.V. Shuvalov (2008). Numerical modeling of emissions for high-speed impact of comets and asteroids on the Moon. *Astron. Vestnik*, V.42, №4, P.351-356.
2. Bazilevskii A.T., A.M. Abdrakhimov, V.A. Dorofeeva (2012). Water and other volatiles on the Moon (review). *Astron. Vestnik*, V.46, №2, P.99-118.
3. Barenbaum A.A. (2002). *Galaxy, Solar system, Earth: Coordinated processes and evolution*. Moscow: GEOS, 393 p. (in Russian).
4. Barenbaum A.A. (2010). *Galactocentric paradigm in geology and astronomy*. Moscow: LIBROKOM, 544 p. (in Russian).
5. Barenbaum A.A. (2012). On the asymmetry surface of the terrestrial planets, caused by the fall of galactic comets. *Vestnik ONZ RAS*, V.4, NZ9001, doi:10.2205/2012NZ_ASEMPG.
6. Barenbaum A.A. (2012a). On the origin of the newest uplifts of Earth crust: new formulation of the problem of global geodynamics. *Uralian Geology Journal*, № 6(90), P.3-26 (in Russian).
7. Barenbaum A.A., M.I. Shpekin (2011). About age of the lunar surface. *Vestnik ONZ RAS*, V.3, NZ6011, doi:10.2205/2011NZ000141.
8. Shevchenko V.V. (1999). On the cometary origin of lunar ice. *Astron. Vestnik*, V.33, №5, P.400-408.
9. Arnold J.R. (1979) Ice in the lunar polar region. *J. Gephys. Res.*, V.84, P.5659-5668.
10. Burke D.J., Dukes C.A., Kim J.H. et al. (2011). Solar wind contribution to surficial lunar water: Laboratory investigations. *Icarus*, V.211, P.1082-1088.
11. Feldman W.C., S. Maurice, D.J. Lawrence et al. (2001). Evidence for water ice near the lunar poles. *J. Gephys. Res.*, V.106, E10, P.2321-23252.
12. Gaddis L.R., C.M. Pieters, B.R. Hawke (1985). *Icarus*, V.61, P.461-489.
13. Head J.W., L. Wilson, (1979). Alphonsus-type dark-halo craters: morphology, morphometry and eruption conditions. *Proc. Lunar and Planet. Sci. Conf.*, V.10, P.2861-2897.
14. Hiesinger H., J.W. Head, U. Wolf, G. Neukum (2001). New age determinations of lunar mare basalts in Mare Cognitum, Mare Nobium, Oceanus Procellarum and other nearside mare. *Lunar and Planet. Sci.*, V.32, Abs. 1815.
15. Housley R.M., R.W. Grant, N.E. Paton (1973). Origin and characteristics of excess Fe metal in lunar glass welded aggregates. *Proc. Lunar. Sci. Conf.*, V.4, P.2737-2749.
16. Housley R.M., E.H.Cirlin, N.E. Paton, I.B. Goldberg (1974). Solar wind and micrometeorite alteration of the lunar regolit. *Proc. Lunar. Sci. Conf.*, V.5, P.2623-2642.
17. McCord T.B., J.Combe (2011). Relationships of widespread OH presence in the lunar surface materials with lunar physical properties. *Lunar and Planet. Sci.*, V.42, Abs. 1843 pdf.
18. McCord T.B., L.A. Taylor, T.M. Orlando et al. (2010). Origin of OH/water on the lunar surface detected by the Moon Mineralogy Mapper. *Lunar and Planet. Sci.*, V.41, Abs. 1860.
19. Ong L., E.I. Asphaug, D. Korycansky, R.F. Coker (2010). Volatile retention from cometary impacts on the Moon. *Icarus*, V.207, P.578-589.
20. Pierazzo E., H.J. Melosh (2000). Hydrocode modeling of oblique impacts: The fate of projectile. *Meteorit. and Planet. Sci.*, V.35, P.117-130.
21. Shpekin M.I. (2009). The Last «Apollo» Orbit Pass over the Tsiolkovsky. *Crater. Intern. Conf.: Astronomy and World Heritage: Across Time and Continents*, Kazan, P.219-221. http://www.ksu.ru/f6/k8/bin_files/ ols138.pdf.
22. Shpekin M.I., R.A. Sitdikova (2007). Topographical survey of Aitken crater on the far side of the Moon. *46-th Vernadsky-Brown Microsymposium*, Moscow, Abs. №46-64.
23. Shpekin M.I., R.A. Sitdikova, A.I. Khairullina (2008). Orbital photogrammetry and laser altimetry of the far side of the Moon in the Aitken crater region. *48-th Vernadsky-Brown Microsymposium*. Moscow, Abs. №150.

Barenbaum A.A. On the mechanism of heating lithosphere rocks by galactic comets

Oil and Gas Research Institute RAS, Moscow

Abstract. We discuss the physical mechanism of heating lithospheric rocks by galactic comets, which includes three steps: 1) aerodynamic destruction of the cometary nucleus with its transformation into a gas stream, 2) formation the shock wave by action this jet which penetrates deep into the lithosphere and causing evaporation, melting and heating of rocks and 3) the modifying of heated rocks column after passage of shock wave. We estimate crater depth, as well as the depth and volume of magma chamber are set up by galactic comets different size. We also considered some tectonic-magmatic phenomena in the Earth's crust and mantle caused by falls galactic comets.

Key words: galactic comets, shock waves, heating mechanism, craters, magma chamber, plumes, intrusives, asthenosphere.

Citation: Barenbaum A.A. (2013). On the mechanism of heating lithosphere rocks by galactic comets.

Introduction. Galactic comets are newly discovered class of large cosmic bodies bombarding the Earth and other planets in the periods when the Solar system is into jet streams of the Galaxy. These comets have speed relative to the Sun about 450 km/s. Diameter their nucleus changes from 100 to 3500, and they preferably consist of water ice density of 1 g/cm^3 [Barenbaum, 2002, 2010]. The consequences such fall comets on the Moon and Mercury, as well as on the Mars with its very tenuous shell, and on the Earth and the Venus are having thick atmosphere, are significantly different. If on planets of first group there are formed craters with a diameter of 10-200 km, then on planets of the second group there are arising seamounts (Earth) and shield volcanoes (Venus) and large areas of surface are raised [Barenbaum, 2012].

The author proposed the mechanism, which explains this phenomenon [Barenbaum, 2013]. According to this mechanism, the interaction of galactic comets with Earth is divided into three stages: 1) the aerodynamic destruction of comet's nucleus in atmosphere and of its conversion into gas stream, 2) the heating of lithosphere rocks by shock wave produced by the fall jet to the surface, and 3) the stage modification of the column heated rocks after passing shock wave. The solution of task on each previous stage is considered as the initial condition of follow-up stage.

1. Comet destruction in atmosphere. As the solution of problems this stage were used the results of [Barenbaum, Shuvalov, 2007], in which we performed the physical-mathematical modeling of the passage through atmosphere the galactic comet with diameter of nucleus

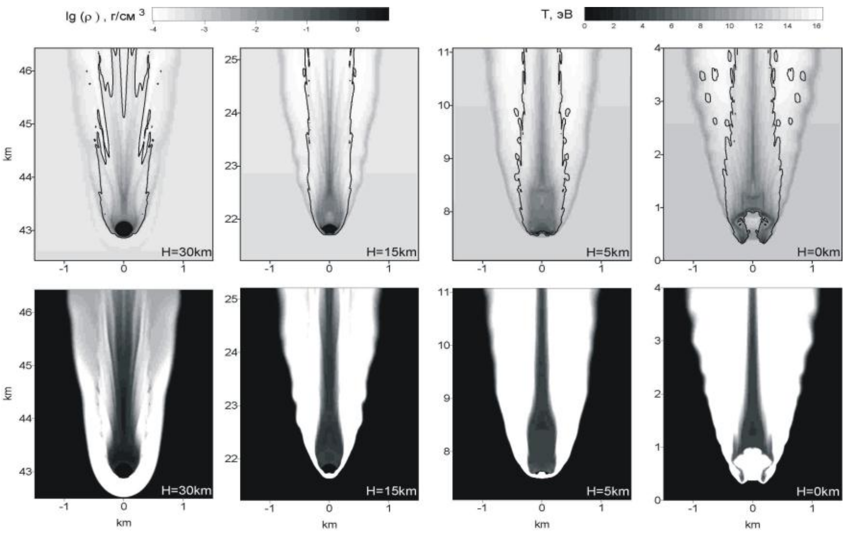

Fig.1

300 m. Calculations lets to trace conversion of icy comet's nucleus at different heights (Fig. 1).

The modeling shown that at an altitude of over 50 km around the cometary nucleus formed a dense cloud of vapor, which slowing down and fills the comet's trail. Before the bow shock wave is formed a warm-layer, thickness of which is several times higher than for cometary nucleus. At altitude of 30 km, due to the emergence of large aerodynamic loads on frontal surface of the nucleus in excess of the limit of the mechanical strength of ice, the cometary nucleus begins to deform and break. Because of the development of the Rayleigh-Taylor instability and Kelvin-Helmholtz instability on the surface of the nucleus appear wavelike disturbances, and it begins to rapidly lose weight. As a result of dispersing the periphery of nucleus and inhibition in air, the mass loss of comet becomes larger than speed evaporation of cometary ice. Growth aerodynamic pressure leads to that on 5-7 km altitude the comet nucleus transforms into crushed pancake structure. Further development of instabilities causes to complete disintegration of cometary nucleus, and at altitudes below 3-5 km, it is converted into the jet consisting of liquid droplet, small solid fragments of nucleus, as well as heated air. At a height of ~ 1 km the jet transforms into stream pure gas. Upon impact, the surface velocity of the jet is different from initial velocity of comet less than 10%.

2. Interaction jet with lithosphere. The solution to this problem we got by using a hydrodynamic model [Lavrentiev, 1959], intended for the theoretical study processes of collisions cosmic bodies moving with very large speed. In accordance with this model, from crash site of jet is begins to spread narrowly focused wave voltage, which gains the energy and momentum of the comet. Penetrating deeply into lithosphere, this shock wave causes strong heating and melting of rocks. Calculations on the Lavrentiev's theory show that after passage of the shock wave in a geological medium is formed the cylindrical canal heavily modified rocks, wherein there are three zones: the top – the zone of evaporation rocks (crater), under it – the zone melting of rocks (magma chamber), and even lower – the heating zone. The results calculations for comets with nucleus diameter $d_к$ = 300 m and 3000 m are shown in Fig. 2 [Barenbaum, 2013].

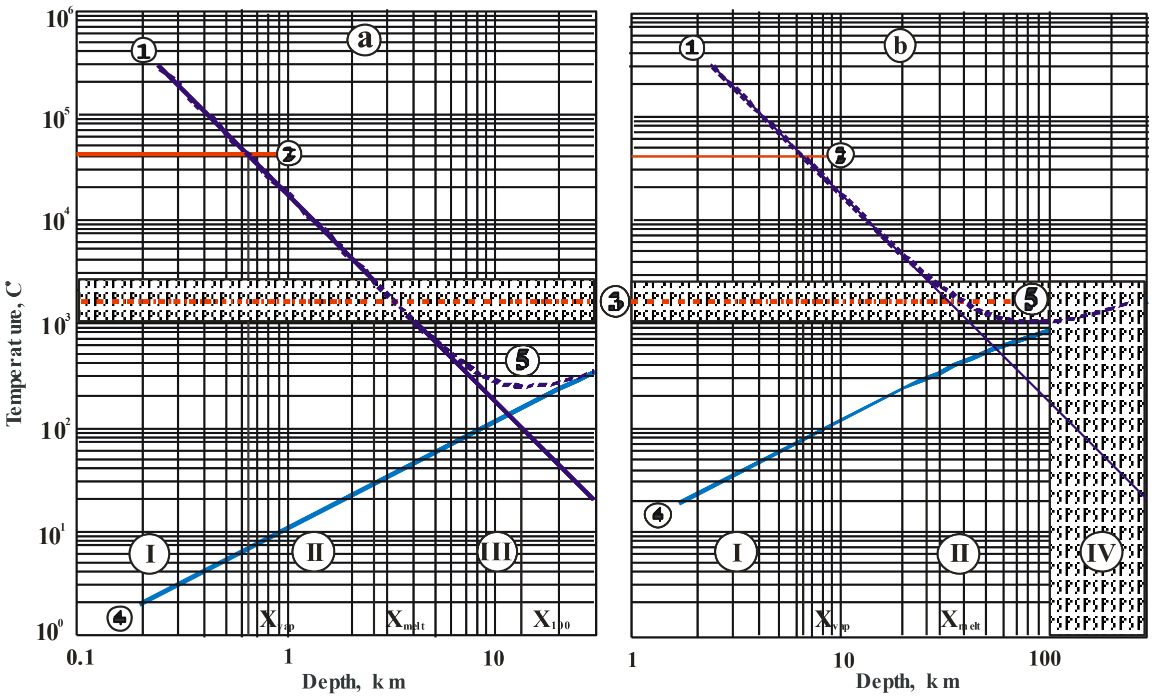

Fig. 2. Heating rocks produced by galactic comets with diameter nucleus of 300 m (a) and 3000 m (b). 1 – the design temperature of heating rocks by shock wave 2 – the evaporation temperature rocks, 3 – range temperature of rocks melting (shaded area), chain line – the average melting point 1750°C, 4 – natural growth temperature of rocks with depth, 5 – the total temperature of heating rocks. Designation zone of rocks: I – evaporation, II – melting, III – heating; IV – asthenosphere

Fig. 2 shows the calculations of depth crater's floor – X_{vap}, depth bottom of magma chamber – X_{melt}, and boundary of rocks heated above 100°C – X_{100}. Diameter column rocks are heated by shock wave is about ~$2d_k$. Dimensions of the zones (I), (II) and (III) correlate to the diameter comet as 2:6:40. For "small" comet the crater has depth and diameter ≈600 m, the magma chamber length ≈2 km, and the length of entire column heated rocks ≈14 km. For "large" comet these estimates increase by 10 times. Resulting length column of heated rocks X_{100} = 140 km reaches the asthenosphere. In this case, the heating caused by shock wave, is summed with natural temperature dependence (4), and the total heating temperature (5) falls within the range of melting rocks (3). The temperature distribution in the column rocks by the shock wave is created per time less than ~1 s.

3. Stage modification. During this stage occupying time from 0.4-2 million years the thermal energy is redistributed between rocks differently heated by shock wave. Calculations show that on modification stage crater completely leveled due to filling molten rock from magmatic chamber located below. Large comet creates melting zone which reaches the asthenosphere. In result is formed a channel through which magma from the asthenosphere can flow out to the surface in an amount far in excess of magmatic chamber volume. Magma that poured out on ocean floor forms seamounts and hotspots, and that crystallized beneath the surface creates intrusions of various types [Barenbaum, 2011]. If total temperature heating (5) lies within the range of melting of rocks, as in Fig. 2b, there is another important effect. It consists in that, that minerals with lower melting after passage of shock wave go into the melt in a certain sequence. Feldspars (T_{melt} = 1100÷1550°C) begin melt in the first queue, pyroxenes (T_{melt} = 1300÷1550°C) follow after them, and olivines (T_{melt} = 1600÷1800°C) in the last queue. Accordingly, after lowering temperature at the final stage of the process these minerals will crystallize from the melt in reverse order.

Discussion of results. We pay attention to other possible consequences of considered mechanism heating lithospheric rocks by galactic comets that can be supported by the available facts.

1. Our hypothesis formation of channels through which magma from the asthenosphere may reach the surface is more acceptable physical explanation of origin hot spots and mantle plumes than well-known today other ideas [Puchkov, 2009]. Petrological data show that magma rises within narrow and long channels by length ~10÷100 km, the mean radius of channels ≈580 m, and the average rate of rise of magma in them ~160 cm/yr [Fedotov, 1976]. According to modern ideas, a basaltic melts are formed at a depth of 100 ÷ 230 km. After that they move to surface through narrow channels and, beginning at depths of 20÷30 km, form magmatic chambers, where can crystallize in form of various intrusions [Sharkov, 1980].

2. According to our estimates, channel of diameter 1÷6 km, connecting the asthenosphere with earth's surface, exists only limited time. If magma is not flowing along the channel, its life time is less of 2 million years [Barenbaum, 2013]. For this time thermal energy of magma is transmitted through the walls channel into the surrounding rocks, causing their heating and partial melting. In that situation magma pillar can break up into system of small magmatic chambers pop-up at the surface. In process of lifting the cameras are deformed, and their rocks are experiencing decompression heating and magmatic differentiation. If thermal energy of the melt is not sufficient, then magma crystallization can lead to origin of all major types of intrusive bodies [Barenbaum, 2011].

3**.** Since heating temperature by shock wave decreases with depth, the magma in the upper part of melting zone is more enriched by high-melting minerals compared with the bottom portion of magma chamber. This fact may explain the existence of two main types of oceanic basalts: tholeiitic and alkaline. It is known [Brown, Massett, 1984] that the tholeiites are usually confined to areas with extremely high temperature gradients (up to 100°C/km) and are formed by partial melting of rocks on small depth. Whereas alkali basalts are formed at greater depths (50–100 km) in areas with lower temperature gradients (up to 30°C/km) and are characterized by lower degree of partial melting mantle rocks.

4. Calculations testify that shock waves from comets with a maximum energy of 1025 J can create considerable heating lithospheric rocks even at depths ~200-250 km. These depths are virtually concur with lower boundary of asthenosphere. Previously we suggested [Barenbaum et al, 2004] that bombardments of the Earth by galactic comets, occurring every 20-37 million years, are the main cause heating of asthenosphere our planet. The results performed calculations can serve as an additional argument in favor of this hypothesis.

Conclusion. The present paper develops the representations [Barenbaum, 2010] that the falls of galactic comets play a decisive role not only in the formation of craters on planets of the Solar system [Barenbaum, Shpekin, 2011, Barenbaum, 2012-a], but also initiate tectonic and magmatic processes on our planet, the causes of which as yet poorly understood. The presented results allow use new approach to the explanation of some of the key to modern geology processes associated with the formation of magmatic chambers, seamounts, hot spots and plumes. The question of origin these geological structures is discussed during last half-century and still unresolved [Puchkov, 2009].

References:

1. Barenbaum A.A. (2002). Galaxy, Solar system, Earth: Coordinated processes and evolution. Moscow: GEOS, 393 p. (in Russian).
2. Barenbaum A.A. (2010). Galactocentric paradigm in geology and astronomy. Moscow: LIBROKOM, 544 p. (in Russian).
3. Barenbaum A.A. (2011). Tectonic and magmatic processes in oceans and on continents as indicators of falls galactic comets. Modern state of the Earth sciences. Intern. Conf. Memory V.E. Hain, Moscow: MSU. http://khain 2011.web.ru. P.166-171 (in Russian).
4. Barenbaum A.A. (2012). On the origin of the newest uplifts of Earth crust: new formulation of the problem of global geodynamics. Uralian Geology Journal, № 6(90), P.3-26. (in Russian).
5. Barenbaum A.A. (2012-a). On the asymmetry of surface terrestrial planets, caused by the falls of

galactic comets. Experiment in GeoSciences, V.18, №1, P.8-11.

6. Barenbaum A.A. (2013). Possible mechanism of heating lithospheric rocks by galactic comets. Uralian Geology Journal, №1(91), p.21-39 (in Russian).
7. Barenbaum AA, VV Shuvalov (2007). Modeling the interaction of galactic comets with atmosphere. Physics of Extreme States of Matter – 2007. Chernogolovka: Institute Problems of Chemical Physics RAS, P.139-140 (in Russian).
8. Barenbaum, A.A., V.E. Hain, N.A. Yasamanov (2004). Large-scale tectonic cycles: the interpretation in the galactic concept position. Vestnik MGU, Ser.4, №3, P.3-16 (in Russian).
9. Barenbaum A.A., M.I. Shpekin (2011). On age of the Moon surface. Bulletin of the Department of Earth Sciences, V.3, NZ6011, doi: 10.2205/2011NZ000141.
10. Lavrentiev M.A. (1959). The problem of penetration at cosmic speeds. Artificial satellites of Earth, Moscow: PH USSR, V.3, P.61-65 (in Russian).
11. Brown G.C., A.E. Massett (1981). The Inaccessible Earth. G.ALLEN&UNWIN, Boston-Sydney.
12. Puchkov V.N. (2009). «The great debate» about the plumes: who is right after all? Geotektonika. №1, P.3-22 (in Russian).
13. Sharkov E.V. (1980). Petrology of the layered intrusions. Leningrad: Nauka, 184 p. (in Russian).
14. Fedotov S.A. (1976). On the mechanism of deep-seated magmatic activity beneath volcanoes of island arcs, and similar structures. Izvestia USSR, Geology, №5, P.25-37 (in Russian).

Kashkarov[1] L.L., Bagulya[2] A.V., Goncharova[2] L.A., Kalinina[2] G.V., Konovalova[2] N.S., Okateva[2] N.M., Pavlova[1] T.A., Polukhina[2] N.G., Starkov[2] N.I., Vladimirov[2] M.S. Determination of the olivine crystals preatmospheric depth position in the Eagle Station meteorite

[1]V.I. Vernadsky Institute of Geochemistry and Analytical Chemistry, RAS, Moscow

[2]P.N. Lebedev Physical Institute, RAS, Moscow

Abstract. On the base of the track-density measuring for about 110 olivine crystals from the Eagle Station pallasite , and using the value of cosmic radiation age of this meteorite, estimated as 300 m.y., it was determined the pre-atmospheric position depth of the meteorite fragment under investigation, which is equal to (4 ± 2) cm.

Key words: galactic cosmic rays, iron-group nuclei, pallasites, track parameters

Citation: Bagulya A.V., L.A. Goncharova, G.V. Kalinina, L.L. Kashkarov, N.S. Konovalova, N.M. Okateva, N.G. Polukhina, N.I. Starkov, M.S. Vladymyrov (2013). Determination of the olivine crystals preatmospheric depth position in the Eagle Station meteorite. *Vestnik ONZ RAN, doi:*

Introduction. Olivine crystals of the Eagle Station pallasite were used as natural track detectors of the nuclei of super heavy (SH) elements of galactic cosmic rays (GCR) [Александров и др., 2008]. The sample of the Eagle Station pallasite is the separate fragment of the meteorite with the size of about 3 × 4 cm, and its space radiation age is estimated at 300 million years. Research is carried out within the framework of the OLYMPIA project [Ginzburg et al., 2004]. One of characteristics of the each olivine crystal, that is used as the natural track detector for determine as the flow of nuclei of super heavy GCR elements registered with the tracks method and also as their energies, is the pre-atmospheric depth position of the analyzed crystals in the meteoroid body.

Research method. To determine the parameters that characterize the depth of the location (position) in the atmospheric meteoroid body of each crystal under investigation, we applied the method based on the measurement of two track parameters of GCR VH-group nuclei (iron-group): bulk track density and their angular distribution in the individual olivine crystals.

Owing to the small size of the Eagle Station sample under investigation (Fig. 1) it is not possibility to measure the position depth of olivine samples in the body of the meteoroid which is due to the character of changes in track density versus pre-atmospheric depth-position of the certain olivine crystals. However, the calculation of the average value of such track-density data using the angular distribution of tracks makes it possible to estimate the some effective crystal position depth from the pre-atmospheric surface of the meteoroid.

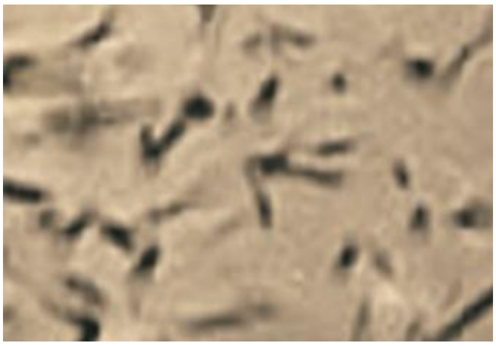

Fig. 1. Photography of the Eagle Station pallasite sample under investigation. The smallest washtub grade is millimeter

Fig. 2. Microphotography of the iron group GCR nuclei etched in one of the olivine crystal from the Eagle Station pallasite meteorite. The track-density equal to $(8 \pm 2)\cdot 10^{6}$ track$\cdot$cm^{-2}. Field size ~ (15 × 25) micron

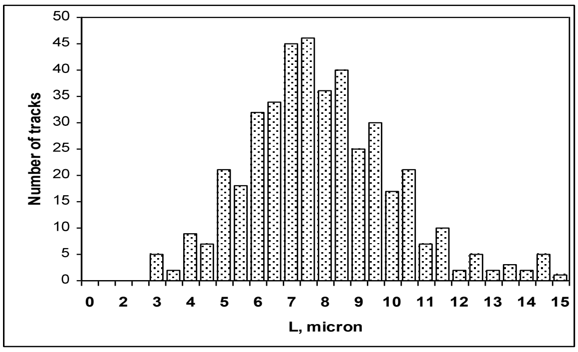

Fig. 3. Statistical track-length (L) distribution of the GCR iron-group nuclei in one of the olivine crystal from the Eagle Station pallasite meteorite.

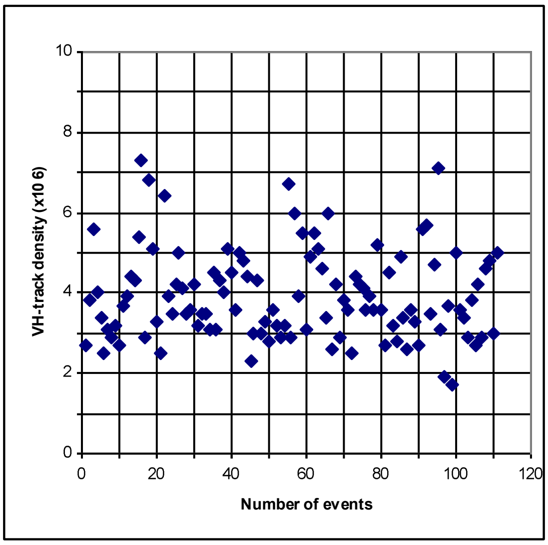

(a)

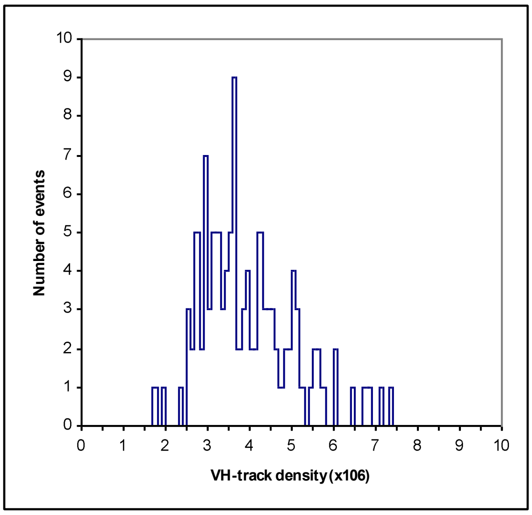

(b)

Fig. 4. Distribution of olivine crystals of the sample of the Eagle Station pallasite under registered track density of the iron group GCR.

Track registering of heavy nuclei in the olivine crystals of pallasites. By their crystallographic structure mineral olivine $(Mg,Fe)_2SiO_4$ silicate relates to silicates with isolated, island position (unlike chain, layered and skeletal silicates) of silicon-oxygen tetrahedra (SiO_4), interconnected with cations Mg or Fe. The individual silicon-oxygen radicals (silicon-radicals) separated from each other. It is expected that due to this structure, the efficiency of chemical etching of the material from the disorders lattice zone along the track braking of heavy nuclei should not strongly depend on the orientation of the tracks relative to the axis of symmetry of the olivine crystal lattice [Егоров и др., 2008]. In addition , it is important to note that the dimensions of the lattice radiation disordering along the trajectory of nuclei braking ten times larger than the unit cell of the crystal: (60÷100) Å compared with the (2-3) Å, respectively. The latter is extremely important confirmation for the problem of registration of the absolute number of relatively short range of tracks from the nuclei of the GCR iron group.

Results. In each olivine crystal under analyze after polishing of their inter-section surface and chemical etching in standard conditions it was measured the track-length (L) values statistical distribution of the GCR iron-group nuclei. Microphotography of the iron group nuclei in GCR composition is shown in Fig. 2 [Kashkarov et al., 2008].

The results of the track-length (L) measuring for iron-group nuclei of GCR are presented in Fig. 3. As it seen, the statistically averaged for ~ 90% of measured tracks value of L is equal to (7.5 ± 2.5) micron. The total observed track-length values are lies in interval from ~ 3 up to ~ 15 micron.

The obtained track-density measured data in 111 olivine crystals under investigation are presented in Fig. 4. At the total interval of the track-density values ~ $(2 - 7)\times10^6$ track·cm^{-2} the overwhelming majority of crystals have the track-density ~ $(4.0 \pm 1.5)\times10^6$ track·cm^{-2}. A very narrow range of variation the track-density values due to small size of the searched meteorite sample, and the shallow depth of its occurrence in the pre-atmospheric body of the meteoroide**Conclusions.** On the basis of the track-parameters measuring for 111 olivine crystals under investigation, and also based on the cosmic radiation age of the Eagle Station meteoroid estimated about 300 m.y., it was determined the position depth of the meteorite fragment under investigation, which is equal to (4±2) cm.

The work was supported by RFBR, grant No 10-02-00375-a, and the Program for Basic Research, RAS, No 22.

References:

1. Alexfndrov A.B., A.V. Bagulya, M.S. Vladimirov et.al. (2008). Method of the charge cosmic ray determination by the track parameters in meteoritic olivine. *Short physic reports FIAN*, V.7, p. 19-27.
2. Egorov V.K., L.L. Kashkarov, N.G. Polukhina, V.A. Tzarev, (2008). Some structural features in the olivine crystals from the Marjalahti meteorite. *Proceedings of the International Workshop "The structure and variety*

of the mineral world", Syktyvkar, Komi Science Centre, p.139-140.

3. Ginzburg V.L., N.G. Polukhina, E.L. Feinberg, N.I. Starkov, V.A. Tsarev (2005). Problems and Horizons of the Search for Tracks of Heavy and Superheavy Nuclei in Olivine Crystals from Meteorites (OLIMPIYA project). *Dokl. Physics*. V. 50. № 6. P. 283–285.
4. Kashkarov L.L., N.G. Polukhina, N.I. Starkov et al., (2008). Geometrical track parameters in the pallasite olivine: identification of the cosmic ray heavy nuclei. *Radiation Measurements*, V.43, p. S266-S268.

Kronrod E.V., Kuskov O.L. Temperature profile of the lunar mantle: agreement with seismic and thermal models

V. I. Vernadsky Institute of Geochemistry and Analytical Chemistry RAS, Moscow

Abstract. This work is about estimation of lunar thermal conditions, surface heat flow values and bulk concentrations of radioactive elements in the Moon. We have suggested the probable temperature profile of the lunar mantle that satisfied geophysical and geochemical constraints and determined possible uranium content in the Moon and surface heat flows.

Key words: Moon, temperature, heat flow, radioactive elements.

Citation: Kronrod E.V., O.L. Kuskov (2013). Temperature profile of the lunar mantle: agreement with seismic and thermal models).

Computer simulation and result. The following issues have been discussed: (1) Estimation of probable temperature distributions in the lunar mantle, (2) Estimation of heat flows and radioactive source intensity.

1 Estimation of probable temperature distribution in the lunar mantle.

Constrains on the temperature profile from seismic velocities**.** We determine the probable temperature from seismic velocities [Gagnepain-Beyneix et al., 2006] inversion temperature profile [Kuskov, O.L., Kronrod, V.A., 1998],[Kuskov O.L., Kronrod V.A., 2009]

The minimal temperature in the upper mantle. The range of probable temperature variations in the mantle was obtained in the works [Kuskov, O.L., Kronrod, V.A., 1998],[Kuskov O.L., Kronrod V.A., 2009]. We have found the minimal temperature in the upper mantle. The minimal temperature of 500^oC at a depth of 150 km satisfies limitations on the mass, moment of inertia and seismic velocities [Kronrod E.V. et al., 2012],[Kronrod V.A. et al., 2011].

The gradient dT/dH in the mantle. Absence of density inversion is a natural requirement for the hydrostatic equilibrium in the satellite. From numerical modeling temperature profile with gradient dT/dH =1.05-0.0006*H, (H – km), was selected. Such a dT/dH gradient satisfies almost zero gradient of density with acceptable accuracy.

The mantle temperature can be described by an equation: $T=1.05*H-0.0003H^2+C$. Temperature gradient at the depth of 150-1000 km accurate within 1^oC, $\delta T_{1000-150} = T_{1000} - T_{150} = 600^o$.

The probable temperature profile. Correlating all of ***constraints on the temperature profile*** we find probable temperature profile of the lunar mantle at the depth less than 1000 km: $T_{pm}{}^oC = 449+1.05*H-0.0003H^2$, H – depth in kilometers.

2 Estimation of heat flows and radioactive source intensity.

To calculate the radioactive source intensity one-dimensional stationary model of thermal conductivity has been used. We propose the following model of the Moon. It consists of the crust, the upper mantle with a heat source Q_{up}, the lower mantle with a heat source Q_{low} and the core. The crust has the depth of 40 km and the density of 2580 kg/m^{-3} [Wieczorek M.A. et al., 2012]. The lower boundary of the upper mantle is within the limits of 500-1000 km depth, the radius of the core is 350 km. The aim of the study is to find values of the heat flow sources corresponding to the set of temperature distribution in the mantle. As a result, the simple analytical relations were obtained. These relations enable to determine the temperature distribution in the mantle. Based on the assumption that Th/U=3.7, K/U=2000 [Hagermann A. et al., 2006], heat conductivity coefficient k=4 W m^{-1}K^{-1}, we have estimated uranium concentration in the upper (C_{Uup}) and lower mantle (C_{Ulow}, $C_{Ulow}= C_{Ubulk}$), surface heat flow (J_s) (Figs. 1, 2) and the corresponding temperature distributions in the lunar mantle (Fig. 3)

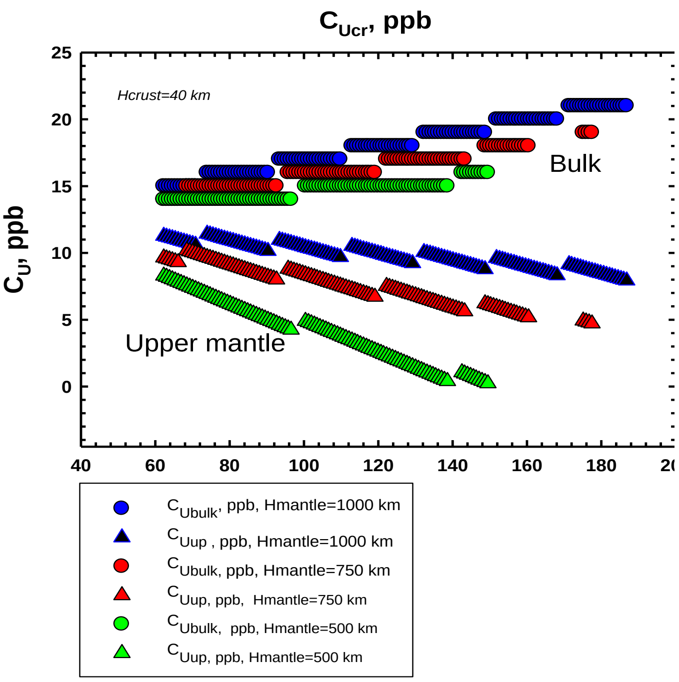

Fig. 1. Calculated uranium concentration in the upper mantle (C_{Uup}) and in the lower mantle (C_{Ulow}, $C_{Ulow}= C_{Ubulk}$). The range of the depth of the boundary between upper and lower mantle H_{mantle} was 500-1000 km, the depth of the crust H_{cr}=40 km, the density of the crust ρ_{cr}=2600 kg/m^3

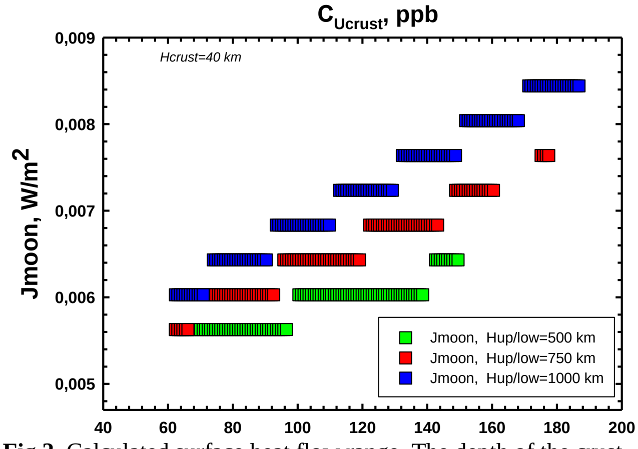

Fig 2. Calculated surface heat flow range. The depth of the crust H_{cr}=40km, the density of the crust ρ_{cr}=2600 kg/m^3

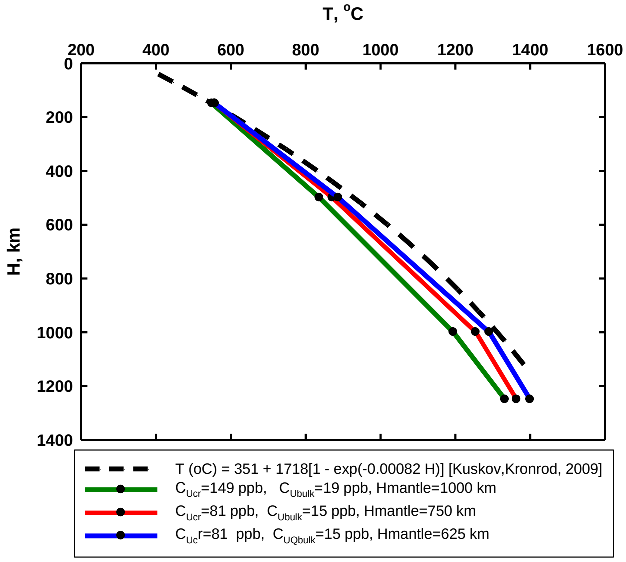

Fig. 3: Temperature distributions in the lunar mantle corresponding to calculated surface heat flow

3. Conclusions

1. We have estimated the acceptable temperature distribution in the lunar mantle which satisfy principal geochemical and geophysical constraints.

2. Assuming that the U concentration in the crust is 150-180 ppb, the estimated bulk lunar U_{bulk} abundances range within 19-21 ppb, upper mantle U_{up} abundances range within 4.7-8.9 ppb, surface heat flow J_{moon}=7.6-8.4 mW/m^2.

Acknowledgements. This research was supported by Russian Academy of Sciences under Programs 22 and 28, and by RFBR grant 12-05-00178 and 12-05-00033.

References:

1. Gagnepain-Beyneix J., P. Lognonné, H. Chenet et al. (2006). A seismic model of the lunar mantle and constraints on temperature and mineralogy. *Phys. Earth Planet. Interiors*, Vol. 159, pp. 140-166
2. Hagermann A., S.Tanaka (2006). Ejecta deposit thickness, heat flow, and a critical ambiguity on the Moon. *Geophys. Res. Lett.*, 33, L19203, doi:10.029/2006GL027030.
3. Kronrod E.V., O.L. Kuskov, V.A. Kronrod (2012). Geochemical and geophysical constraints for thermal field of the Moon. *EPSC Abstracts*, Vol. 6, EPSC-DPS2011-16.
4. Kronrod V.A., O.L. Kuskov (2011). Inversion of Seismic and Gravity Data for the Composition and Core Sizes of the Moon. *Izv. Phys. Solid Earth.*, Vol 47, pp. 711-730.
5. Kuskov O.L., V.A. Kronrod (1998). Constitution of the Moon: 5. Constraints on composition, density, temperature, and radius of a core *Phys. EarthPlanet. Interiors*, Vol. 107, pp. 285-306.
6. Kuskov O.L., V.A. Kronrod (2009). Geochemical constraints on the model of the composition and thermal conditions of the Moon according to seismic data. *Izv. Phys. Solid Earth.*, Vol. 45, pp. 753–768
7. Wieczorek M.A., Neumann, G.A., Nimmo, F. et al. (2012). The Crust of the Moon as Seen by GRAIL. *Sciencexpress*, http://www.sciencemag.org/content/early/recent/5 December 2012 / Page 1/ 10.1126/science.1231530.

Shornikov S. I. A thermodynamic study of genesis of «white inclusion» substance in meteorites

V. I. Vernadsky Institute of Geochemistry and Analytical Chemistry RAS, Moscow

Abstract. Within the framework of the developed semi-empirical model based on the theory of ideal associated solutions, thermodynamic calculations were made of changes in the «white inclusions» substance composition in meteorites during their evaporation and condensation. Our examination of the data presented by Grossman et al. showed their fundamental internal discrepancy. The most typical for the evaporation processes of «white inclusions» substance in meteorites is a considerable change in the ratio of magnesium and silicon oxides contents $x(MgO)$ / $x(SiO_2)$ at a constant ratio of calcium and aluminum oxide contents $x(CaO)/x(Al_2O_3)$.

Key words: thermodynamics of evaporation, the CaO–MgO–Al_2O_3–SiO_2 system, «white inclusions» in meteorites.

Citation: Shornikov, S. I. (2013). A thermodynamic study of genesis of «white inclusion» substance in meteorites, *Vestn. Otd. nauk Zemle*, 4, (doi:).

The problem of forming the substance of «white inclusions» in meteorites known in the literature as CAI (Ca–Al–Inclusions) has been attracting researchers' attention for a long time. The composition of these inclusions is quite heterogeneous (mass %): SiO_2 (25–35), CaO (24–33), Al_2O_3 (6–33), MgO (7–21), FeO (1–3), TiO_2 (1.0–1.5) and can be approximately considered within the framework of the CaO–MgO–Al_2O_3–SiO_2 oxide system.

Almost 40 years ago Grossman formulated the theory of consecutive condensation of nebular matter [Grossman, 1972]. Over the last decade Grossman et al. within the framework of this theory, has been modeling the high-temperature CAI evaporation process in order to determine the composition of its predecessors and requirements for their formation [Ebel & Grossman, 2000; Grossman et al., 2008]. The results obtained by Grossman et al. determined the purpose of the present study, which is to carry out thermodynamic calculations of changes in the composition of «white inclusions» in meteorites during their possible evaporation and condensation. Particular attention was accorded to the problem of changes in the ratio of magnesium and silicon oxides contents $x(\mathrm{MgO}) / x(\mathrm{SiO_2})$ in these processes, which we to some extent considered earlier [Shornikov, 2012].

Let us consider the procedures of thermodynamic calculations of changes in the composition of the «white inclusions» substance in meteorites during their possible evaporation and condensation used by Grossman et al. in comparison to those used in the present study (table 1).

1. It seems wrong to use the Hertz-Knudsen equation in the form chosen by Grossman et al. [Grossman et al., 2008] because the authors found it possible, in the absence of any data on the CAI substance condensation, to consider them equal to its evaporation coefficients.

2. Earlier [Shornikov, 2008] we already considered in detail and criticized the evaporation coefficient values found in nonequilibrium thermodynamic conditions accepted by Grossman et al. Let us note that, in his calculations of the evaporation coefficient, Hashimoto [Hashimoto, 1983] used simultaneously the data related to both nonequilibrium and equilibrium thermodynamic conditions.

3. The calculation of Grossman et al. of partial pressures based on the system of the balance equations set up in terms of stoichiometric relationships for partial pressures of gas phase components over the CAI substance is not quite correct and was also criticized [Shornikov, 2009]. It is shown that stoichiometric relationships p_i / p_j at any value $p_{\mathrm{O_2}}$ for all gas phase components are not realized.

4. The models *Melts* [Ghiorso et al., 1983] and *CMAS* [Berman, 1983] used by Grossman et al. have also been criticized in detail earlier [Shornikov, 2009]. It is shown that, within the framework of the regular solutions theory of the underlying the *Melts* model, it is impossible in a satisfactory manner to calculate equilibriums with participation of solid phases of the $\mathrm{CaO–MgO–Al_2O_3–SiO_2}$ system. In the case of the *CMAS* model, restrictions are caused by the application of the semi-empirical Margules equation, which requires a significant number of experimental data in a wide interval of temperatures and concentrations to calculate the parameters that describe the melt.

5. As regards the source thermochemical data [Robie et al., 1978] used in both aforementioned models, we have also discussed them for a typical case of magnesium silicates – enstatite and forsterite [Shornikov, 2013]. It is shown that the systematic deviation (towards a Gibbs energy of compound formation increase, which is identical for both enstatite and forsterite – approximately by 2.5 kJ/mole) is caused by the integration procedure of the parametric heat capacity equation for calculating the Gibbs energy of compound formation in the high temperature region.

6. The correctness of the thermodynamic approach developed by Grossman et al. [Ebel & Grossman, 2000; Grossman et al., 2008] has not been verified. The reliability of the approach proposed in the present study is shown on the example of available experimental data. Comparison of the results obtained in the present study with the experimental data obtained by the Knudsen effusion mass spectrometry method [Markova et al., 1986] shows their satisfactory conformity.

Table 1. The comparison of calculation procedures used by Grossman et al. [Ebel & Grossman, 2000; Grossman et al., 2002; Grossman et al., 2008] and in the present study.

Calculation procedure	Grossman et al.	The present study
1. The Hertz-Knudsen equation	$$J_e = \frac{\alpha(p_{tot} - p_{env})}{\sqrt{2\pi RTM_i}}$$ J_e – the melt evaporation speed, α – the evaporation (condensation) coefficient, p_{tot} – the total vapour pressure, p_{env} – the environment vapour pressure, R – the gas constant, T – the temperature, M_i – the melt molecular weight; The evaporation and condensation coefficients of liquid phases are less than 1; The evaporation coefficient was accepted as equal to condensation coefficient.	$$J_e = \frac{\alpha p_{tot}}{\sqrt{2\pi RTM_i}}$$ J_e – the melt evaporation speed, α – the evaporation coefficient, p_{tot} – the total vapour pressure, R – the gas constant, T – the temperature, M_i – the melt molecular weight; The evaporation coefficients of liquid phases was accepted equal 1; The condensation coefficient was not considered; The environment vapour pressure was considered in item 3.
2. The evaporation coefficients	The nonequilibrium experimental thermodynamic data [Hashimoto, 1983].	The mass spectrometric experimental data [Shornikov, 2003].

Calculation procedure	Grossman et al.	The present study
3. The calculations of partial pressures	The system of the balance equations. For a case of oxygen pressure: $p_{O}^{tot} = p_{CaO}^{tot} + p_{MgO}^{tot} + 1.5 p_{Al_2O_3}^{tot} + p_{SiO_2}^{tot}$	The system of the equations using the equilibrium constants of reactions [Glushko et al., 1978–1982]
4. The calculations of oxide activities	The model *Melts* [Ghiorso et al., 1983; Ebel & Grossman, 2000] in frames of theory of regular solutions; The model *CMAS* [Berman, 1983; Grossman et al., 2008] according to Margules parametrical equation.	The semi-empirical model [Shornikov, 2009] in frames of theory of ideal associated solutions.
5. The initial thermodynamic data	The thermochemical data [Robie et al., 1978]	The mass spectrometric experimental data [Shornikov, 2003]
6. The comparison of calculation results with the experimental data	It has not been verified.	The check of coincidence of the calculations [Shornikov & Yakovlev, 2010] with the experimental data [Markova et al., 1986].

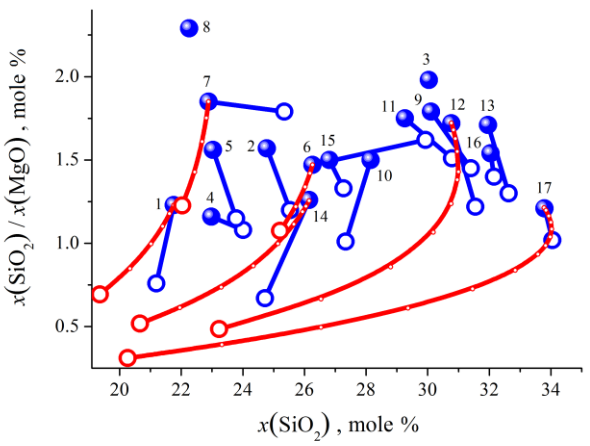

Fig. 1. The predecessors' compositions of CAI substance calculated by Grossman et al. [Grossman et al., 2008] and in the present study. Table of symbols: the predecessors of CAI substance are designated by not painted over symbols, the examples of CAI substance are designated by painted over symbols; the results of Grossman et al. are blue, the results of the present study are red; the numbers designated the composition numbers in [Grossman et al., 2008].

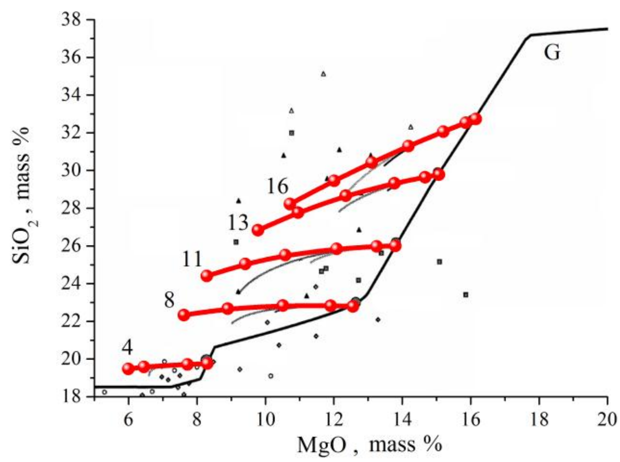

Fig. 2. The composition changes of $CaO–MgO–Al_2O_3–SiO_2$ melts being on curve condensation at evaporation calculated by Grossman et al. [Grossman et al., 2002] and in the present study.
Table of symbols: the condensation curve is designated by a symbol G; the results of Grossman et al. are represented by black lines, the results of the present study are represented by red lines; the number designated the sample mass losses at evaporation determined in the present study; various dot symbols represented the observed compositions of CAI substance.

The predecessors' compositions calculated by Grossman et al. [Grossman et al., 2008] in accordance with the above procedures, from which appropriate CAI substance samples could be formed by evaporation, are shown in fig. 1 in comparison with those calculated in the present study.

In fig. 1 the inconsistency of calculations of Grossman et al. [Grossman et al., 2008] can be easily seen. Thus, for example, two similar compositions (No. 6 and No. 15) have absolutely different predecessors. At the same time, the presence of a common predecessor in absolutely different compositions (No. 4 and No. 5; No. 6 and No. 11) is inexplicable. Apparently, such results are a consequence of Grossman's calculation procedures discussed above.

The same reasons probably explain the observable differences between the calculation results showing changes in the compositions on the condensation-at-evaporation curve obtained by Grossman et al. [Grossman et al., 2002] and the present study results (fig. 2). According to calculations of Grossman et al., evaporation of silicon dioxide from the melt occurs quite quickly, which contradicts the experimental data [Markova et al., 1986].

Thus, within the framework of the developed semi-empirical model based on the theory of ideal associated solutions [Shornikov, 2009], thermodynamic calculations were made of composition changes in the «white inclusions» substance in meteorites during their evaporation and condensation. Our examination of the data presented by Grossman et al. [Ebel & Grossman, 2000; Grossman et al., 2002; Grossman et al., 2008] showed their fundamental internal discrepancy. The calculations made in the present study revealed regularities in the evaporation of «white inclusions» substance typical for all the compositions studied. The most typical for the evaporation and condensation processes of «white inclusions» substance in meteorites is a considerable change in the ratio of magnesium and silicon oxides contents $x(MgO) / x(SiO_2)$ at a constant ratio of calcium and aluminum oxide contents $x(CaO) / x(Al_2O_3)$.

Acknowledgments. I am grateful to prof. Igor V. Kaspin (Herzen State Pedagogical University of Russia, Saint-Petersburg) for technical assistance.

References:

1. Berman, R. G. (1983). A thermodynamic model for multicomponent melts, with application to the system $CaO–MgO–Al_2O_3–SiO_2$, Vancouver: Univ. British Columbia, 153 pp.
2. Ebel, D. S., L. Grossman (2000). Condensation in dust-enriched systems, *Geochim. Cosmochim. Acta*, vol. 64, no. 2, pp. 339–366.
3. Ghiorso, M. S., I. S. E. Carmichael, M. L. Rivers, R. O. Sack (1983). The Gibbs free energy of mixing of natural liquids; an expanded regular solution approximation for the calculation of magmatic intensive variables, *Contrib. Mineral. Petrol*., vol. 84, no. 1, pp. 107–145.
4. Glushko, V. P., L. V. Gurvich, G. A. Bergman, I. V. Veitz, V. A. Medvedev, G. A. Khachkuruzov, V. S. Youngman (1978–1982). Thermodynamic properties of individual substances, M.: Nauka.
5. Grossman, L. (1972). Condensation in the primitive solar nebula, *Geochim. Cosmochim. Acta*, vol. 36, no. 5, pp. 597–619.
6. Grossman, L., D. S. Ebel, S. B. Simon (2002). Formation of refractory inclusions by evaporation of condensate precursors, *Geochim. Cosmochim. Acta*, vol. 66, no. 1, pp. 145–161.
7. Grossman, L., S. B. Simon, V. K. Rai, M. H. Thiemens, I. D. Hutcheon, R. W. Williams, A. Galy, T. Ding, A. V. Fedkin, R. N. Clayton, N. K. Mayeda (2008). Primordial compositions of refractory inclusions, *Geochim. Cosmochim. Acta*, vol. 72, no. 12, pp. 3001–3021.
8. Hashimoto, A. (1983). Evaporation metamorphism in the early solar nebula – evaporation experiments on the melt $FeO–MgO–SiO_2–CaO–Al_2O_3$ and chemical fractionations of primitive materials, *Geochem. J.*, vol. 17, no. 3, pp. 111–145.
9. Markova, O. M., O. I. Yakovlev, G. A. Semenov, A. N. Belov (1986). A some general experimental results on evaporation of natural melts in Knudsen cell, *Geokhimiya*, no. 11, pp. 1559–1569 (in Russian).
10. Robie, R. A., B. S. Hemingway, J. R. Fisher (1978). Thermodynamic properties of minerals and related substances at 298.15 K and 1 bar (10^5 Pascals) pressure and at high temperatures, *U. S. Geol. Surv. Bull.*, no. 1452, 456 pp.
11. Shornikov, S. I. (2003). Thermodynamic properties of the melts and vapors of the $CaO–MgO–Al_2O_3–SiO_2$ system determined by the mass spectrometric study, *Vestnik Otdelenia nauk o Zemle RAN*, vol. 21, no. 1, http://geo.web.ru/conf/khitariada/1-2003/informbul-1_2003/magm-10e.pdf.
12. Shornikov, S. I. (2008). Effect of redox conditions on the evaporation of oxide melts in the $CaO–MgO–FeO–Al_2O_3–SiO_2$ system, *Geochem. Int.*, vol. 46, no. 7, pp. 724–729.
13. Shornikov, S. I. (2009). Investigation of abilities of thermodynamic approaches on calculations of oxide activities in the compounds of the $CaO–MgO–Al_2O_3–SiO_2$ system, *Vestnik Otdelenia nauk o Zemle RAN*, vol. 27, no. 1, http://onznews.wdcb.ru/publications/asempg/planet-33.pdf (in Russian).
14. Shornikov, S. I., O. I. Yakovlev (2010). High-temperature thermodynamic study of the condensed phase composition changes of CAI substance at evaporation, *Proc. XVI Russian meeting on experimental mineralogy*, pp. 289–291 (in Russian).
15. Shornikov, S. I., O. I. Yakovlev (2010). A study of CAI melt composition changing during evaporation, *Lunar Planet. Sci. XXXXI*, abstract no. 1408.
16. Shornikov, S. I. (2012). Thermodinamics of evaporation and condensation of CAI substance, *Proc. XIII intern. conf. «Physico-chemical and petrophysical researches in Earth sciences»*, pp. 299–302 (in Russian).
17. Shornikov, S. I. (2013). Thermodynamic properties of $MgO–SiO_2$ system: experimental data and calculations, *Proc. the scientific seminar devoted to scientific activity of prof. I. L. Khodakovsky*, pp. 223–230 (in Russian).

Yakovlev[1] O.I., Dikov[2] Yu.P., Gerasimov[3] M. V., Buleev[2] M.I. Cluster vaporization of feldspars in the conditions of impulse heating

[1]Vernadsky Institute of Geochemistry and Analytical Chemistry RAS, Moscow

[2]Institute of Raw Deposits, Petrography, Mineralogy and Geochemistry RAS, Moscow

[3]Space Research Institute RAS, Moscow

Abstract. New experimental data are presented that confirm cluster vaporization type in the conditions high temperature impulse heating. The experiments were carried out on plagioclase feldspars: $Ab_{91}Ort_5An_4$, $Ab_{43}Ort_5An_{52}$, $Ab_{30}Ort_1An_{69}$, $Ab_{18}Ort_1An_{81}$ and orthoclase feldspar - $Ab_{51}Ort_{38}An_{11}$. The analyses of vapor-condensate phase using X-ray photo-electronic spectroscopy permit to discover some cluster forms similar to nepheline, wollastonite, sillimanite, quarts and corund.

Key words: vaporization, condensation, impact process, impulse heating.

Citation: Yakovlev O.I., Yu.P. Dikov, M. V. Gerasimov, M. I. Buleev (2013). Cluster vaporization of feldspars in the conditions of impulse heating

The study of cluster type vaporization is necessary for understanding the problem of the global chemical differentiation at impact-accretionary stage of our planet. As we know the chemical change of high temperature impact melt is the result of selective vaporization. The main regularities of this process in the equilibrium conditions are rather well known [Markova et al. 1986]. However the vaporization of exactly impact melts may be described by cluster type one. The cluster type vaporization is characterized by transition into vapor phase of the large atomic-molecular group or blocks. The cluster mechanism of vaporization does not baffle all theoretical description so far, and at the current time it is necessary to collect experimental data.

In this publication we present new experimental results on cluster vaporization of a number feldspar: albite $Ab_{91}Ort_5An_4$, Na-labrador $Ab_{43}Ort_5An_{52}$, Ca-labrador $Ab_{30}Ort_1An_{69}$, bitovnite $Ab_{18}Ort_1An_{81}$ and ortoclase $Ab_{51}Ort_{38}An_{11}$. Chemical analytical data permitted to give the conventional name to observed clusters. They were similar to the famous mineral minal name. For cluster determination we use special method which consists of laser impulse vaporization, vapor quench condensation, layer-by-layer analyses by X-ray photo electron spectroscopy (XPS) and measurements of energy bonding of 2p electrons of Si, Ca, Al in the condensate layers.

Impulse vaporization of minerals was carried out using laser installation. The duration of the laser pulses was 10^{-3} s, and the energy density was 10^6 to 10^7 W/cm^2. At such parameters of the laser pulses, the samples were heated to temperatures of 4000–5000°C. A sample to be studied (in the form of a crystal) was mounted in the hermetically sealed chamber 500 cm^3 in inner volume. The focused radiation of the Nd laser (d = 3–4 mm) passed through an optical glass of fused quartz and impact the sample. The total air or He pressure in the cell was 1 atm. A Ni foil (screen) was placed at a distance of 5–8 cm from the target at the expansion pathway of the vaporized cloud, and the vapor condensed on the foil in quenching regime. The estimated time of vapor travel from the target to foil was 10^{-5} s, which is notably lower than the duration of the laser pulse itself and ensured the layer by layer accumulation of the condensate simultaneously with the current vaporization of the target. Each individual condensate layer thus had a chemical composition and atomic–molecular state corresponding to those of the current vapor portion. In turn, the whole vertical section of the condensate layers provided information on the vaporization succession of the target during the time it was affected by the laser pulse. The thicknesses of the condensate layers accumulated in the experiments varied from 200 to 10000Å.

The chemical analyses of the starting samples and condensate films were analyzed by XPS. The condensate films were abraded layer by layer by Ar ions at a step of ~100–200 Å, and each layer was analyzed by XPS. This ensured the structural and chemical completeness of the analysis throughout the whole vertical section of the condensate layer. The position of components of the spectral line was determined with accuracy ± 0.02 eV. The errors in the analyzed concentrations of individual elements were ±5% at concentrations >10 at %, and lower concentrations (<10 at %) were analyzed with accuracy ± 10%. X-ray photoelectron analysis allowed us to determine, along with the elemental composition of the condensate, also the bonding energy values of the elements and their valence states.

The important way for cluster forms identification and cluster type vaporization is comparison data of binding electron energy of elements in condensate and the binding energy similar electrons in reference book for elements in already studied minerals and compounds [Dikov et al., 1979; Warner et al., 2010; Anderson, Swartz, 1974].

Table. Binding energy of internal electrons of Si, Al и Ca in silicate and oxides (eV)

Minerals	Si2p	Al2p	Ca2p	Reference
Nepheline	102.2 ± 0.1	74.7 ± 0.1		Dikov et al., 1979
Wollastonite	102.36 ± 0.02		347.04 ± 0.02	Warner et al., 2012
Sillimanite	102.8± 0.1	74.8± 0.1		Anderson, Swartz, 1974
Corund		74.2 ÷ 74.6		Warner et al., 2012
Quartz	103.3 ÷ 104.0			Warner et al., 2012
SiO	100.4 ÷ 102.0			Warner et al., 2012

In the table there are shown the reference data of binding energy of Ca, Si and Al in the minerals which we used for identification of clusters in the condensate layers. The experimental results as well as the results for cluster identification are presented in fig.1 and 2. The figures show the standards binding energy for elements in some minerals (between parallel lines), depth of the condensate layer and experimental measurements.

The figures clearly show that the condensate consists of atomic-molecular group (clusters) and the measured binding energy data of Si2p electrons correspond to compounds SiO_2, Al_2SiO_5, $CaSiO_3$ and $NaAlSiO_4$.

Short format of this paper does not permit us to show the whole materials of our experiments. That is why we shall restrict our self by short comments onto our results. The cluster identification conducted not only by energy data of Si2p electrons but also by Al2p and Ca2p electrons. Their were discovered that impulse vaporization of albite formed quarts, sillimanite and nepheline clusters; vaporization of orthoclase - nepheline and wollastonite clusters; vaporization of Na-labrador - nepheline and wollastonite clusters; vaporization of Ca-labrador - nepheline, quarts and wollastonite clusters; vaporization of bitovnite - nepheline, wollastonite, sillimanite, quarts and corund. It is interesting to note that the condensates in some experiments consisted fully of cluster forms. For example the condensate from Ca-labrador experiment consisted of nepheline, quarts and wollastonite clusters in proportion of ~ 35:55:10.

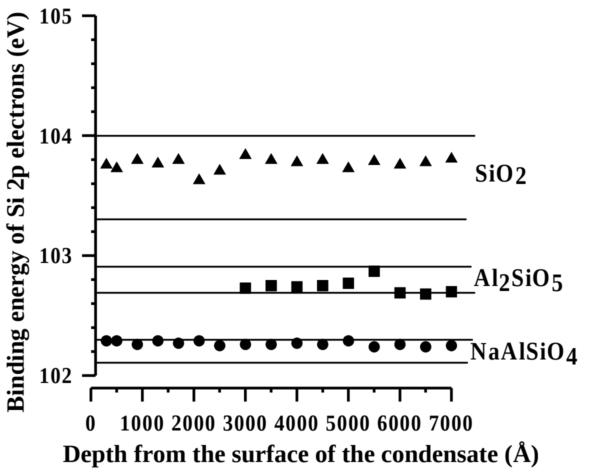

Fig.1. The observed binding energy of Si2p electrons in the condensate layers which were obtained at albite vaporization and comparison these date with date of reference book for SiO_2, Al_2SiO_5 and $NaAlSiO_4$.

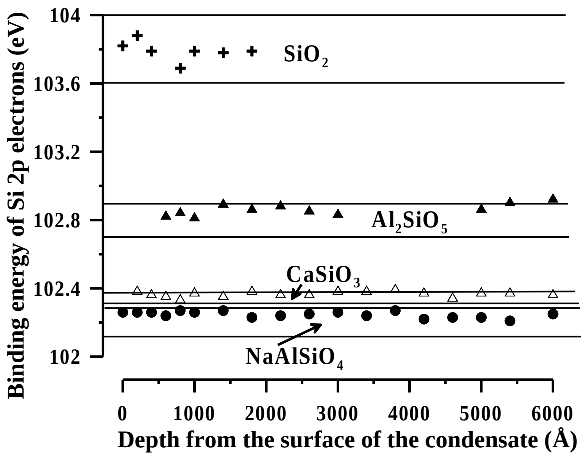

Fig.2. The observed binding energy of Si2p electrons in the condensate layers which were obtained at bitovnite vaporization and comparison these date with date of reference book for SiO_2, Al_2SiO_5, $CaSiO_3$ and $NaAlSiO_4$.

What is the mechanism of cluster origin? We suggest that initial clusters formed in high temperature melts during fast heating process and melting of minerals. At high temperature state minerals step by step dissociated into complicated molecules which transposed in vapor state. Then these complicated molecules (clusters) quenched in the processes of vapor expansion and condensed on metallic plate keeping initial cluster forms. The thermodissociation processes during impulse heating was probably slower than vaporization processes. As the result, in vapor phase could appear the stable structural mineral fragments. This mechanism of cluster origin is most probable. It has been confirmed by thermodynamic calculation which we conducted using "Magma" program [Fegley, Cameron, 1987]. The program permits to determine possible stable atomic-molecular mineral group in the melts at 2500-4500^{o}C. The results of calculations showered that at high temperatures in the feldspar melts stable atomic-molecular group - nepheline, sillimanite and wollastonite presented indeed.

Cluster vaporization mechanism could play important role in element distribution between vapor and melt phases in impact processes as the clusters could combine the elements or oxides whose individual volatility differ drastically (e.g. nepheline cluster which contents high volatile Na_2O and low volatile Al_2O_3). In this case the usage of classical row of elements or oxides volatility [Markova et al. 1986] for interpretation of residual impact melt and condensate compositions may lead to mistakes.

References :

1. Warner C.D., A.V. Naumkin, A. Kraut-Vass, J.W. Allison et al. (2010). *NIST X-ray Photoelectron Spectroscopy Database* (NIST Standart Database 29, Version 3.5), http://srdata.nist.gov/xps/
2. Dikov Yu.P., I.A. Britov, Yu.P. Romashenko, S.P. Dolin (1979). Peculiarities of electronic structure of silicates, Nauka Press, Moscow, 127 p.
3. Anderson P.R., W.E. Swartz (1974). X-ray Photoelectron Spectroscopy of Al_2SiO_5 *Inorganic Chemistry,* №. 13, p. 2293.
4. Fegley B. Jr., A.G.W.Cameron (1987). A vaporization model for iron/silicate fractionation in the Mercury protoplanet. *Earth and Plenet. Sci. Lett*., v. 82, p. 207-222.
5. Markova O.M., O.I. Yakovlev, G.A. Semenov, A.N. Belov (1986). Some general results of experiments on vaporization of natural melts in Knudson chamber. *Geokhimiya*, No 11, p. 1559–1569..

Ivliev A.I., Kuyunko N.S. Thermoluminescence in Ash Creek and Tamdakht chondrites

V. I. Vernadsky Institute of Geochemistry and Analytical Chemistry RAS, Moscow

Abstract. Thermoluminescence was examined in the fres-fallen Ash Creek (L6) and Tamdakht (H5) chondrites. The experimental information were used to study the shock-thermal of the chondrites, and the sizes of their orbits.

Key words: thermoluminescence, chondrites, metamorphism.

Citation: Ivliev A.I., N.S. Kuyunko (2013). Thermoluminescence in Ash Creek and Tamdakht chondrites.

INTRODUCTION. The Tamdakht (H5) and Ash Creek (L6) meteorites discussed herein belong to the most widely spread H and L groups of ordinary chondrites, which account for approximately 70% of the total number of meteorite falls. The Ash Creek chondrite fell in the morning of February 15, 2009, witnessed by numerous onlookers, not far from the town of West (for which the meteorite was originally named) in McLennan County, Texas, United States. The fall was videotaped from the town of Austin, at a distance of 180 km from the fall site and was also traced by two radars. The chondrite is classed with ordinary chondrites of L6 group, shock stage S3 [Weisberg, 2009a].

The Tamdakht meteorite fell on December 20, 2008, in Morocco, in a mountainous terrain between Marrakesh and Ouarzazate, not far from the village of Tamdakht. The falling body likely had a high velocity, and very few of its undamaged fragments were preserved. The chondrite is classed with ordinary chondrites of H5 group, shock stage S3 [Weisberg, 2009b].

A universal process that formed meteorites as individual cosmic bodies was collision, and one of the most sensitive techniques applicable in studying shock metamorphism is thermoluminescence (TL).

EXPERIMENTAL. The Ash Creek (L6) and Tamdakht (H5) meteorites are equilibrium ordinary chondrites, whose TL provides insight into the character of their shock metamorphism and make it possible to quantify the sizes of their orbits [Sears, 1988]. Our data on the TL "stored" during the irradiation of samples in the laboratory (TL_{IND}) in oligoclase, quartz, and calcite affected by various shock pressures in our experiments led us to conclude that the significant variations in the intensity of TL_{IND} were caused [Ivliev, 1995, 1996, 2002], first of all, by various grades of shock metamorphism of the meteorites but not by differences in the TL characteristics of feldspar, a mineral contained in all H, L, and LL chondrites in roughly equal proportions and having roughly similar composition in these meteorites ($Ab_{74}An_{20}Or_6$) [Dodd, 1981]. Our TL data on more than 30 meteorite samples confirm this conclusion [Ivliev, 2008]. It was demonstrated that the intensity of TL_{IND} increases with increasing shock pressure in equilibrium ordinary chondrites of shock stages S1 and S2 and decreases with the transition from shock stage S3 to S6. These data were utilized to derive formulas for evaluating shock pressure that affected the meteorites at their collisions in space.

In order to evaluate the perihelia of the orbits of the Ash Creek and Tamdakht meteorites, we have measured their TL accumulated in space (TL_{NAT}), whose intensity can be controlled (in the opinion of the authors of the method [Melcher, 1981]) by certain characteristics of the orbits. Obviously, the smaller the perihelion, the higher the temperature to which the meteorite body is heated and, accordingly, the lower the stored TL_{NAT}. To conduct the calculations, we normalized TL_{NAT} of each sample to its sensitivity by measuring the TL_{IND} per dose unit induced by the radiogenic source. This ratio, which is referred to as the equivalent dose (ED) can be calculated for a certain temperature value on the glow curve as:

$$ED = D\,(TL_{NAT}/TL_{IND}), \qquad (1)$$

where D is the radiation dose of the meteorite in the laboratory. The reader can find more detailed descriptions of the ED technique in our earlier papers [Ivliev, 1995, 1996, 2002, 2006]. The ED value calculated for TL luminesce at 250°C lies within 200-1500 Gy (20-150 krad) for most ordinary chondrites whose fall dates are known, and this corresponds to perihelion values of ~0.8 - 1.0AU [Melcher, 1981].

The methods applied for sample preparation and TL measurements are analogous to those described in [Ivliev, 1995, 1996, 2002]. It is only pertinent to mention that the meteoritic material was utilized to prepare three 2 mg samples of each meteorite. The TL values were calculated from the averages of the three measurements.

Figure 1 shows the glow curves obtained by recording the TL of the samples of the Ash Creek and Tamdakht chondrites, and the numeral *1* denotes the TL_{NAT} glow curves, *2* corresponds to TL_{IND} induced by X-ray radiation, and *3* marks TL_{IND} induced by gamma-radiation from ^{137}Cs. It should be mentioned that the radiation dose of Ash Creek was 1.49 kGy, and that of Tamdakht was 3.12 kGy. As was mentioned above and in [Ivliev, 2008], the TL_{IND} intensity increases with the transition from the shock stage S1 to S2 and decreases with the transition from the shock stage S3 to S6. For the shock stages S1 - S2, the shock pressure *P* was calculated by the formula:

$$P = 1.93 \times \ln(S_P) - 5.57, \qquad (2)$$

and that for the shock stages S3 - S6 by the formula:

$$P = -12.28 \times \ln(S_P) + 91.74, \qquad (3)$$

where P is GPa, and S_P is the TL_{IND} intensity induced by X-ray radiation, whose value is calculated as the surface below the glow curve within the sample heating region of 40 - 350°C. In order to elucidate as to which of the formulas (2) or (3) is more suitable for the calculations, one can use the results of petrographic studies. Our preliminary results indicate that the shock stage of meteorites can be identified in certain instances from measured TL_{NAT}.

Figure 2 shows TL_{NAT} glow curves of meteorite samples of various shock stages: Bjurboeole L4, S1 (glow curve 1); Nikol'skoe L4, S2 (*2*); Pultusk H5, S3 (*3*); and Dalgety Downs L4, S4 *(4).* It can be readily seen that the TL_{NAT} intensities for meteorites of different shock stages are also notably different: the maximum height of the peak is typical in the Nikol'skoe meteorite of shock stage S2 (curve *2).* The TL_{NAT} of Bjurboele (shock stage S1) is less intense, and the further transition to shock stages S3 and S4 is accompanied by the decrease in the TL_{NAT} intensity (curves *3* and *4* for the Pultusk and Dalgety Dawns meteorites). The comparison of the TL_{NAT} glow curves in Fig. 1 (curves *3)* with the glow curves in Fig. 2 led us to classify the Ash Creek and Tamdakht meteorites with shock stage S2. This implies that the shock pressure that affected the meteorites in space should be calculated by formula (3). The calculations yielded the following shock pressure values: 15 ± 2GPa for Ash Creek and 20 ± 2 GPa for Tamdakht. The evaluated shock pressures classify these meteorites with shock stage S3, which is consistent with the estimates from petrographic data [Weisberg, 2009a,b].

As was mentioned above, the perihelia of the orbits of the meteorites can be estimated from the equivalent dose ED (see formula (1)). The authors of this technique of perihelion evaluation [Melcher, 1981] suggested that values should be calculated at a certain TL glow temperature (250°C). Our TL measurements in three samples prepared from the material of a single meteorite indicate that the error in the ED values calculated by this technique is often higher than 25%. Our method for the calculation of ED from the TL intensity at sample heating to temperatures of 240 - 340°C makes it possible to reduce the measurement error to ~ 10% and even less. Our calculations yielded the following values: ED = 600 ±10 Gy for Ash Creek and ED = 1.2 ± 0.1 kGy for Tamdakht. As was demonstrated in [Melcher, 1981], such *D* values correspond to the perihelion region typical of most meteorites: 0.8 - 1 AU.

This work is supported in part by the Program No. 22 of Fundamental Research of Russian Academy of Sciences and Program No. 4 ONZ of Russian Academy of Sciences.

References:

1. Dodd R.T. (1981). Meteorites. A Petrologic_Chemical Synthesis. University Press, Cambridge. Cambridge, 368 p.
2. Ivliev A.I., D.D. Badyukov, and L.L. Kashkarov (1995). Study of Thermoluminescence in Samples Subjected to Experimental Shocked Samples. I: Oligoclase. *Geokhimiya*, № 9, P. 1368–1377.
3. Ivliev A.I., D.D. Badyukov, and L.L. Kashkarov (1996). Investigations of Thermoluminescence in Experimentally Shocked Samples: II. Quartz. *Geokhem. Int.*, № 34, P. 912–919–1018.
4. Ivliev A.I., D.D. Badyukov, N.S.Kuyunko, and E.A.Kozlov (2002). A Study of Thermoluminescence in Experimentally Shocked Samples. III: Calcite. *Geochem. Int.*, № 40, P.739–750.
5. Ivliev A.I., V.A. Alexeev (2006). Estimation of the meteorite orbits by the thermoluminescence method. *Lunar Planet. Sci. XXXVII.* Houston. CD-ROM, #1047.pdf.
6. Ivliev A.I., N.S. Kuyunko (2008). The study of ordinary chondrites by the thermoluminescence method. *Lunar Planet. Sci. XXXIX*. Houston. 2008. CD-ROM, #1053.pdf.
7. Melcher C.L., R.M. Walker (1981). Thermoluminescence and meteorite orbits. *Earth Planet. Sci. Lett.*, v. 52, № 1, p. 39–54.
8. Sears D.W.G. (1988).Thermoluminescence of meteorites: Shedding light on the cosmos *Nucl. Tracks Radiat. Meas.*, v. 14, № 1/2, p. 5–17.
9. Weisberg M.K., C. Smith, G. Benedix, Ch.D.K. Herd, K. Righter, H. Henning Haack, A. Yamaguchi, H. Chennaoui

Aoudjehane and J.N. Grossman (2009a). The Meteoritical Bulletin, No. 96, *Meteoritics Planet. Sci.*, v. 44, № 9, p. 1355-1397.

10. Weisberg M.K., C. Smith, G. Benedix, L. Folco, K. Righter, J. Zipfel, A. Yamaguchi, H. Chennaoui Aoudjehane (2009b). The Meteoritical Bulletin, No. 95. *Meteoritics Planet. Sci.*, v. 44, № 3, p. 1–33.

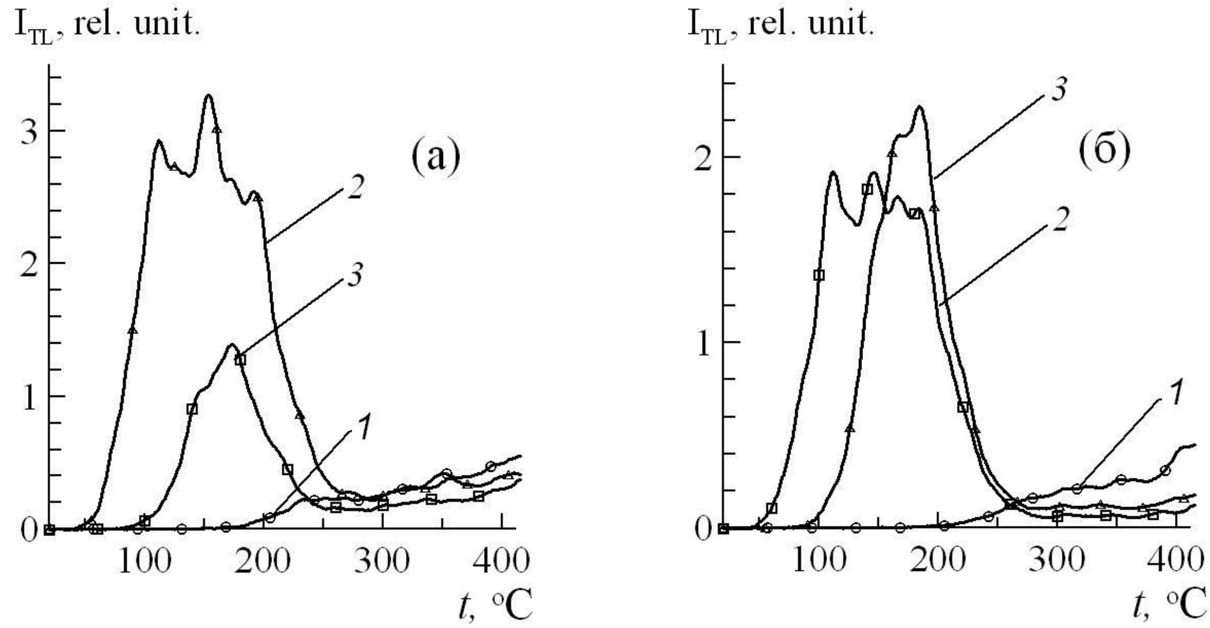

Fig. 1. Glow curves of the (a) Ash Creek and (b) Tamdakht chondrites due to natural TL_{NAT} (line *1*) and TL_{IND} induced by (*2*) X-ray and (*3*) gamma-radiation; I_{TL} is the TL intensity expressed in relative units, t is the heating temperature of the sample.

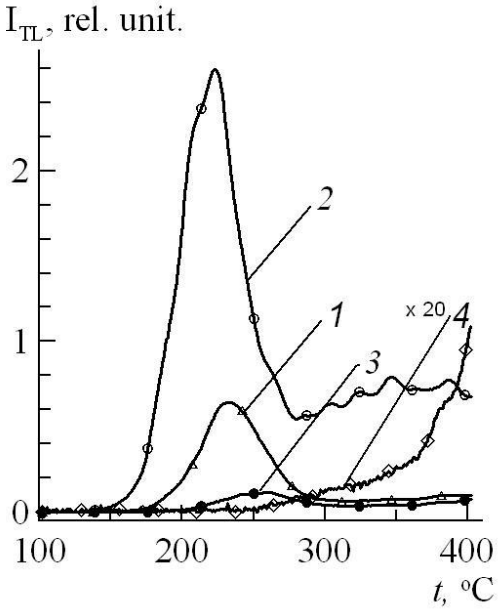

Fig. 2. Glow curves obtained by registering natural TLNAT in the Bjurboele (line *1*), Nikolskoe (*2*), Pultusk (*3*), and Dalgety Downs (*4*) meteorites. The ITL values of (4) are shown in the diagram 20 times greater.

Kashkarov L.L., Kalinina G.V., Pavlova T.A.
Thermal annealing of charge particle tracks in silicate and phosphate minerals for investigation of the radiation-thermal meteorite history

V.I. Vernadsky Institute of Geochemistry and Analytical Chemistry, RAS, Moscow

Abstract. The results of the track method analyse in silicate (olivine) and phosphate (apatite) minerals from chondrites are considered in the problem of chondrite-matter thermal-history investigation. The main basic positions are the next: 1) the presence of different charge particles, chiefly there are solar cosmic ray (SCR) iron-group nuclei and (Th,U)-fission fragments; 2) different ability to store the tracks of charge particles depending on the temperature and duration of heating for various minerals. By comparing the data of track analysis a quantitative estimate of the upper threshold temperature heating of the meteorite during the interval of time elapsed since the start of the accumulation tracks was performed. The detection of tracks from the nuclei of the iron group of SCR in olivine crystals seen primarily as an undoubted fact of irradiation of crystals on pre-accretion or regolith stage of formation of the meteorite parent body.

Key words: tracks, iron-group nuclei, solar cosmic rays, fission fragments, chondrites, apatite, olivine.

Citation: Kashkarov L.L., G.V. Kalinina, T.A. Pavlova (2013).Thermal annealing of charge particle tracks in silicate and phosphate minerals for investigation of the radiation-thermal meteorite history. *Vestnik ONZ RAN, doi:*

Introduction. The matter of meteorites is characterized by a degree of pressure and thermal (heat) reworking. The main characteristics used to describe the extent of this impact are: the structural, petrological and chemical characteristics. However, radiation effects such as the formation of tracks along the trail braking of heavy charged particles, can be extremely useful for considering of the history of the meteoritic matter formation. In particular, for the matter of ordinary chondrites it can be observed the traces of radiation exposure related to the early history of their parent bodies formation, since before the accretion phase.

Methods research. The main provisions in the study of the thermal meteorites history are as follows: 1) The presence of different kinds of charged particles among them for silicate minerals the major nuclei are the iron group nuclei of solar cosmic rays (SCR), and for the phosphates are the ^{238}U isotope fission fragments, included into the compound of this mineral enriched by this element. 2) Different ability to store the tracks in the specified minerals.

Based on the comparison of the data track analysis of crystals of phosphates and silicates, in the work is carried out the quantitative estimate of an upper threshold temperature heating of the meteoritic material during the total interval of time since the beginning of the track accumulation. In this case, the tracks in the phosphate crystals are accumulated, starting with the cooling time of the meteorite parent body to the temperature of the keeping of braking traces of the ^{238}U fission fragments. Tracks from the heavy elements nuclei of cosmic rays under the irradiation of unprotected matter in accretion state (stage) or in the regolith state on the surface of the meteorite parent body, in the absence of further strong heating of matter, are collected and saved since the moment of their formation beginning.

The discovering of such tracks in silicate minerals, which are the track detectors, is considered as an indisputable fact, firstly, of the exposure of some part of meteorite matter at an early stage of its parent body formation of the given meteorite, and the second, the absence of the long thermal, or short-term shock-thermal event in the meteorite history, which could lead to the extinction of these tracks.

From the graph shown in Fig. 1, it follows that the penetration depth of the iron group nuclei of the cosmic rays with energies of (10 - 100) MeV/nucleon in the chondrites matter does not exceed a thickness of several hundred microns. This means that either the irradiating matter is in the finely divided state (submillimeter grain size), or there were irradiated the larger particles subsequently subjected to fragmentation.

The results of an experimental study of the tracks annealing in the Eagle Station pallasite olivine crystals [Goswami et al., 1984], given on the Fig. 2 (a), have shown that at the sufficiently high temperatures (400-500 ° C) almost all the tracks of the iron group cosmic rays nuclei accumulated by the time of heating in the olivine crystal disappear completely within a very short period of time (see Table 1).

As it is seen on the Fig. 2 (b), the storage of tracks in the olivine crystals, which located at the lower temperature (below ~50 ° C), up to several tens of percent over longer time intervals (tens and hundreds of million years).

The dependence of the storage degree of the ^{238}U fission fragments tracks from the duration and the annealing temperature from the apatite (merrillit) crystals of the Estacado meteorite [Gleadov, Duddy, 1981] is presented on the Fig. 3.

As it is apparent from the figure 3, the complete (full) healing of the ^{238}U fission fragments tracks occurs at the temperature of about 450 ° C during 60 minutes of annealing. Obviously, at the higher temperature heating of the apatite (500 °C or higher) tracks are completely disappear in a few minutes.

Thus, the above results of the thermal analysis of tracks storage in the olivine and apatite crystals indicate on the possibility to estimate as the maximum temperature of the full annealing of tracks so on the effective value of the heating temperature of these minerals for a long time.

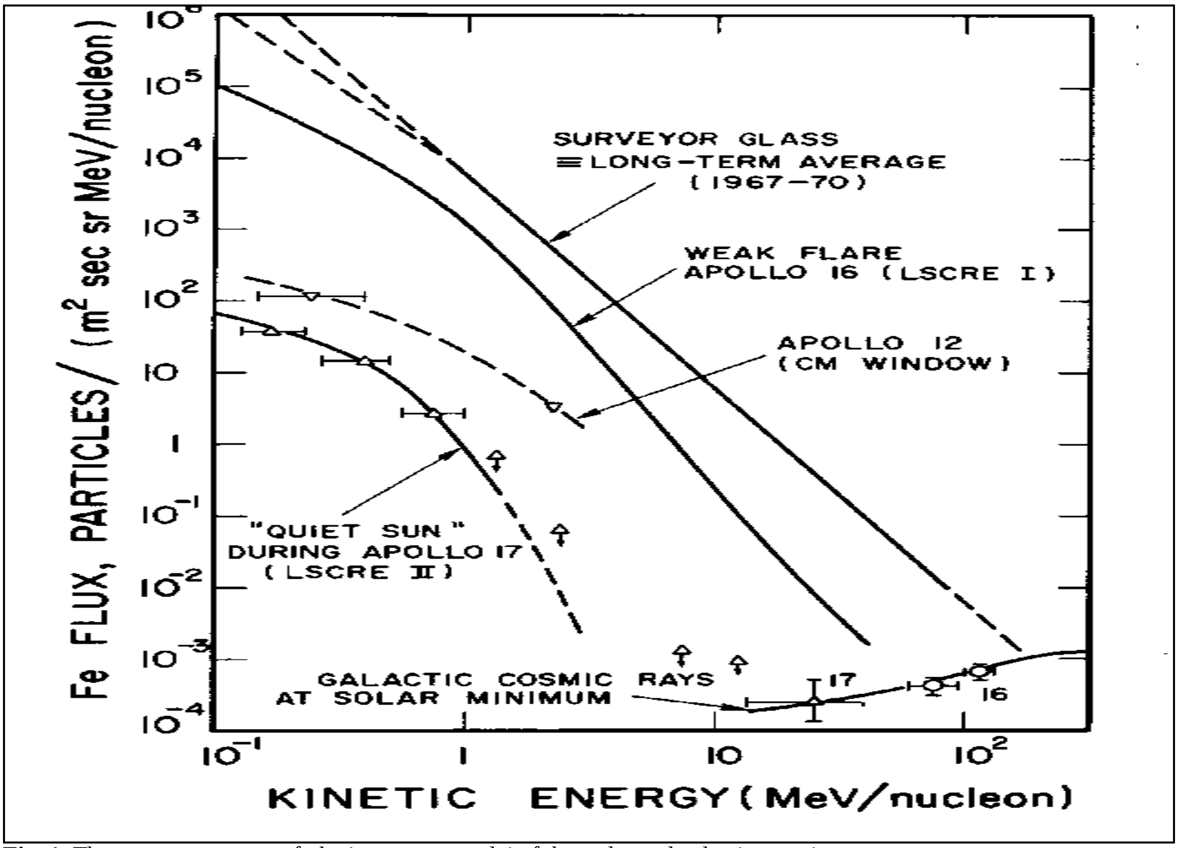

Fig. 1. The energy spectrum of the iron group nuclei of the solar and galactic cosmic rays.

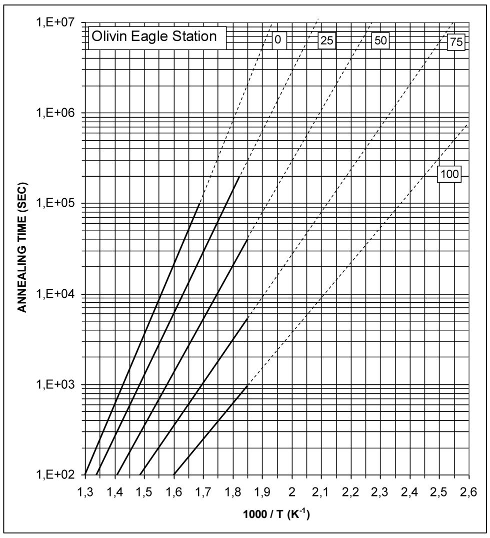

(a)

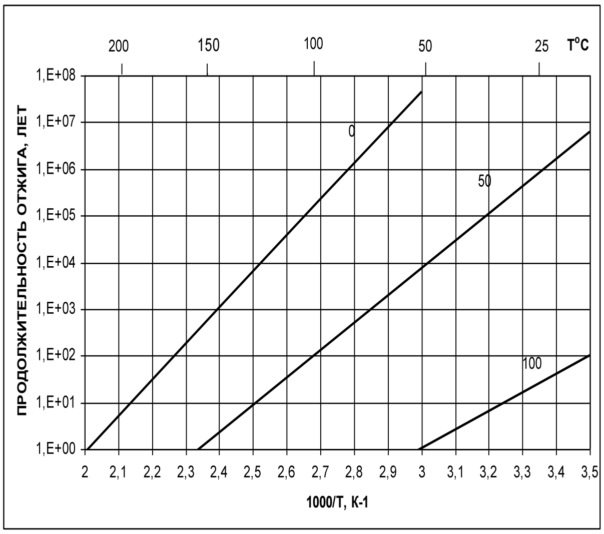

(b)

Fig. 2. The dependence of the annealing degree of the iron group SCR nuclei tracks in olivine crystals from the Eagle Station pallasite at the different temperatures and the annealing time according to: (a) experimental data; and (b) the extrapolation analysis.

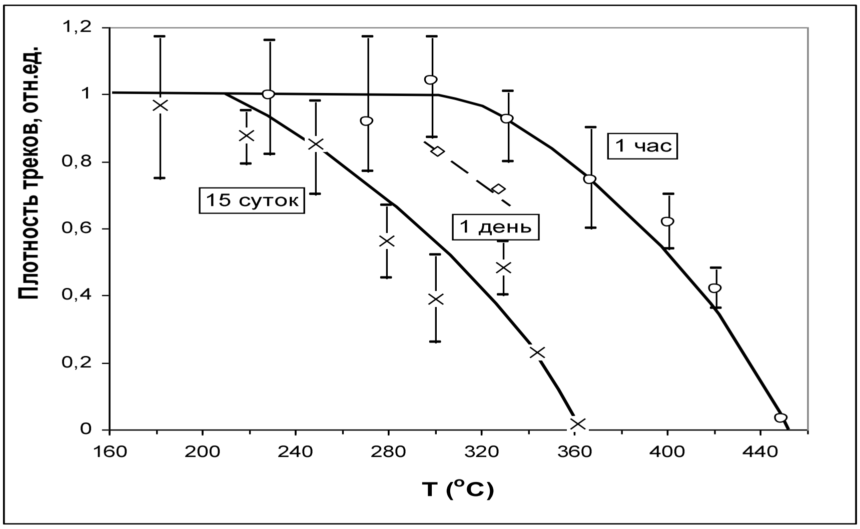

Fig. 3. The changing of the tracks density of ^{238}U fission fragments on the annealing temperature of apatite (merrilita) from the Estacado meteorite for different time intervals.

Table 1. Time intervals of the tracks annealing (minutes) in the olivine crystals from the Eagle Station pallasite at different temperatures**.**

Keeping of tracks, %	Temperature, °C		
	500	400	300
0	1 .7	55	1833
25	0 .8	20	433
50	0 .4	6	88
75	0 .2	2	17
100	0 .1	0,6	4

Conclusions. The dependence of the storage degree of the tracks formed by the iron group nuclei of the SCR (very high track density and track density gradient observed from the surface into the deep of the individual mineral grains) and the galactic cosmic rays (uniform in the volume of each individual crystal relatively low density of tracks) in the olivine crystals, and also of the fission fragments of heavy elements in the phosphate crystals, on the duration and the annealing temperature allow to carry out the quantitative indicative assessment of the time-temperature parameters of the thermal meteohondrits history.

The degree of tracks storage is determined by their geometric parameters compared with the parameters of the newly tracks induced in the same crystals.

The parameters of the thermal history of the meteorite matter obtained from the track data analysis for the different minerals, that are part of the given meteorite matter, lead to the significant refinement of the results.

The work is supported by the Program for Basic Research, No 22.

References:

1. Gleadov A.J.W. and I.R. Duddy (1981). A natural long-term track annealing experiment for apatite. *Nucl. Tracks*, 5, 169-173
2. Goswami J.N., R. Jha and D. Lal (1984). Quantitative treatment of annealing of charge particle tracks in common minerals. *Earth and Planet. Sci. Lett.*, 71, 120-128.

Lebedev E.B.[1], Roschina I.A. [1], Kononkova N.N. [1], Zevakin E.A. [1], Averin[2] V.V **Influence of physico-chemical conditions on division of the iron-sulfide and silicate phases in partial molten melt**

[1]V.I.Vernadsky Institute of Geochemistry and Analytical Chemistry RAS, Moscow

[2]A.A.Baykov Institute of metallurgy and material science RAS, Moscow

Abstract. The modeling is carried out on a high-temperature centrifuge at temperatures 1440-1460ºC and in the controlled conditions of oxygen potential. Calculations of the values of oxygen fugacity were also performed on the basis of chemical composition of the phases of the quenched samples after the experiments.

Key words: experimental study, magmatic melts, metallic phases, accumulation, segregation, oxygen fugacity.

Citation: Lebedev E.B., I.A.Roschina, N.N.Kononkova, E.A.Zevakin, V.V Averin (2013). Influence of physico-chemical properties on division of the iron-sulfide phases in partial molten melt. *Vestnik ONZ RAN.*

Geochemical criteria of the Moon's composition as deficient in Fe and depleted in volatile components and the distribution of siderophile elements in the planet offer the possibility of correlating, under certain conditions, the origin of the Moon and its core from an initial material of composition close to CI carbonaceous chondrites. Mechanisms of formation of the Moon's metallic core may be associated with the model of the percolation of liquid metallic Fe through a silicate matrix. The question arises whether the segregation of metal is possible under such low degrees of melting. In order to verify the model of the percolation of liquid metallic Fe through a silicate matrix of chondritic composition at low degrees of melting, we have experimentally modeled Fe movement and deposition in the course of high-temperature centrifugation. In our experiments, Fe was segregated in systems with Fe sulfide and silicate melts at partial melting under reduced conditions and the deformation of the silicate framework.

Most hypotheses dealing with metal segregation during the early evolution of planets assume the separation of the metallic phase from the silicate liquid, and physico-mathematical models of percolation processes proceed from this assumption. It is thus important to consider a model of Fe segregation in heterogeneous multiphase systems with multiple grains of silicate minerals, first of all, olivine.

However, the dynamics of magmatic differentiation is complicated, and it is so far uncertain as to which are conditions of Fe precipitation at the minimum degree of melting (less than 10%) of peridotite rocks if the melt contains 5% Fe and a low concentration (less than 5%) S. Our modeled composition of Fe–S metal corresponds to 95% Fe, 5% S, and minor P–Si–C amounts, which improve the casting characteristics of Fe (viscosity, interfacial tension, and wettability of phases).

With regard for the considerations presented above, we selected the composition of the metallic phase according to the model suggested for the origin of the Moon's and its core from a material at the calculated concentrations of Fe in the core (5%) and a degree of partial melting of <13%.[Galimov, 2004]

In order to model the conditions of Fe segregation in the course of partial melting, we applied high-temperature centrifugation [Lebedev, Galimov, 2012].

The experimental setup consisted of an original centrifuge with 3000–6000 rpm and a revolution radius of 11 cm. The ampoule with the sample was ~1 cm long and made it possible to increase gravity in the sample by factors of 2000-4000; the temperature was T = 1400–1500°C, and oxygen fugacity was approximately five logarithmic units below the IW buffer.

The experiments were carried out with the aim of elucidating the physicochemical conditions (minimum degree of melting of ultramafic rocks with a deformed silicate framework) needed for the percolation and deposition of Fe sulfide (Fe–S) phases through a silicate matrix of peridotite composition at a specified and varied oxygen fugacity.

Figures 1 exhibit the Fe precipitate after centrifugation in our experiment CS-110. The composition f the starting mixture was 85% Ol, 10% ferropicrite, and 5% Fe–S (95% Fe and 5% S). The experimental parameters were 4000 g gravity acceleration, T = 1440°CC, t = 15 min, ceramic (ZrO2) ampoule, C–CO buffer (diluted), W casing, Δ log fO2 (IW) = –(5.5 ± 0.2). The load weight was 1.5 g and exerted pressure immediately on the sample from above (Fig. 1,).

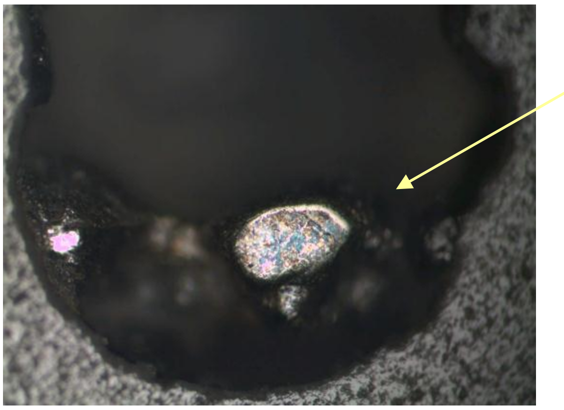

Fig. 1. Experiment CS-110. Fe precipitate (1a).

Conclusions

1. High-temperature centrifugation was utilized to experimentally model Fe segregation at a low S concentration (no more than 5%) in systems of Fe sulfide and silicate melts under highly reduced conditions of approximately five logarithmic units below the IW buffer and temperatures of 1400–1440°C, simultaneously with the partial melting and deformation of the silicate framework under a pressure and with the flow of the metal toward a zone of lower pressure.

2. The mechanical deformation of the silicate framework during centrifugation is proved to be associated with Fe percolation and precipitation from a mixture of olivine crystals, mafic silicate melt, and Fe sulfide melt at low degrees of partial melting.

3. This result proves that the Moon could be produced from a primary peridotite material of composition close to CI carbonaceous chondrites.

This work was supported by RFBR Grant 07-05-00630 and Grant Program of the Presidium of RAS № 24

References:

1. Galimov E. M. (2004). On the Origin of Lunar Material. Geochemistry International, Vol. 42, No. 7, pp. 595–610.
2. Lebedev, E.B., E.M. Galimov (2012). Experimental Modeling of the Origin of the Moon's Metallic Core at Partial Melting. Geochemistry International, Vol. 50, No. 8, 639–648